Rapid Changes in Risk Preferences Originate from Bayesian Inference on Parietal Magnitude Representations

Gilles de Hollander[1], Marcus Grueschow[1], Franciszek Hennel[2], Christian C. Ruff[1]

1. Zurich Center for Neuroeconomics, Department of Economics, University of Zurich, Zurich, Switzerland
2. Institute for Biomedical Engineering, University of Zurich and ETH Zurich, Zurich, Switzerland

Abstract

Risk preferences – the willingness to accept greater uncertainty to achieve larger potential rewards – determine many aspects of our lives and are often interpreted as an individual trait that reflects a general 'taste' for risk. However, this perspective cannot explain why risk preferences can change considerably across contexts and even across repetitions of the identical decisions. Here we provide modelling and neural evidence that contextual shifts and moment-to-moment fluctuations in risk preferences can emerge mechanistically from Bayesian inference on noisy magnitude representations in parietal cortex. Our participants underwent fMRI while choosing between safe and risky options that were either held in working memory or present on the screen. Risky options that were held in working memory were less likely to be chosen (risk aversion) when they had large payoffs but more likely to be chosen (risk-seeking) when they had small payoffs. These counterintuitive effects are mechanistically explained by a computational model of the Bayesian inference underlying the perception of the payoff magnitudes: Options kept in working memory are noisier and therefore more prone to central tendency biases, leading small (or large) payoffs to be overestimated (or underestimated) more. Congruent with the behavioural modelling, fMRI population-receptive field modelling showed that on trials where intraparietal payoff representations were noisier, choices were also less consistent and less risk-neutral, in line with participants resorting more to their prior belief about potential payoffs. Our results highlight that individual risk preferences and their puzzling changes across contexts and choice repetitions are mechanistically rooted in perceptual inference on noisy parietal

magnitude representations, with profound implications for economic, psychological, and neuroscience theories of risky behaviour.

Corresponding authors: Gilles de Hollander (Gilles.de.Hollander@gmail.com); Christian C. Ruff (christian.ruff@econ.uzh.ch)

Keywords: Risk aversion, Bayesian cognition, Number Sense, Neural encoding models

Running Title: Risk Preferences Originate from Bayesian Perception

N. figures and Tables: 4 figures, 0 tables

Competing Interests The authors declare no competing financial interests.

Acknowledgements: We are grateful to C. Schnyder, K. Treiber and M. Moisa at the Zurich Center for Neuroeconomics for their excellent assistance in recruitment and participant facilitation. C.C.R. received funding from the University Research Priority Program 'Adaptive Brain Circuits in Development andLearning' (grant no. URPP AdaBD) at the University of Zurich and the Swiss National Science Foundation (grant no. 100019L-173248). G.d.H.was funded by the Dutch Research Council NWO (Rubicon grant no. 019.183SG.017/8O3B) and the University of Zurich (Forschungskredit grant no. K-33153-02-01)

Introduction

A central pillar of decision theory is that people make different choices because they have different underlying preferences. For example, some might take more risks for the chance of bigger rewards, whereas others might not[1–9]. In real life, this might mean that some people are more willing than others to become self-employed, engage in relationships, or to invest money in the stock market[10]. Classic choice theories explain such individual differences as varying preferences for larger over smaller gains that are described by characteristics of individual utility functions[3,4,11]. According to this view, preferences reflect the extent to which a decision-maker favors choice options over others based on their subjective evaluation of risk and reward. This concept of (risk) preferences is used throughout many scientific fields, including household economics[12], consumer behaviour[13], game theory[3], health economics[14], environmental economics[15], finance[16], social decision-making[17], macroeconomics[18,19], and psychology[9,20]. Furthermore, the field of neuroeconomics, which studies the neural underpinnings of economic behaviour, often takes this perspective of preferences as a starting point for analyzing neural data, e.g., by looking for neural correlates of subjective value that guide observed choices under uncertainty[21–23].

Although some theorists[24] distinguish between risk preferences (defined by observed choice in a given choice set) and risk attitudes (a broader psychological trait that describes a person's general appetite or distaste for taking risks), many standard decision theories equate risk preferences with attitudes, because the former are mathematically tractable. Moreover, they assume that such preferences are stable over time[2,13] and largely similar across people: "[O]ne does not argue about tastes for the same reason that one does not argue over the Rocky Mountains—both are there, will be there next year, too"[2]. Accordingly, most economic theories say very little about where risk preferences come from or why they are the way they are.

However, empirical data reveal that risk preferences are, unlike the Rocky Mountains, highly variable[25,26]. First of all, they seem to depend on context. For example, objectively identical choice sets (i.e., accept/reject a certain gamble) can lead to different choices depending on the options that were offered before[27] or in which order choice options are presented[28]. Moreover, it is routinely found that even when the exact same choice problem is presented repeatedly throughout an experiment within the same context, participants still choose differently across repetitions[7,29,30]. Such choice stochasticity has been addressed in random utility theory (RUT) by adding a random noise term to classic utility functions[31,32]. However,

although RUT alleviates the problem of choice inconsistency, it ultimately fails to address the question of where this noise originates from, or why risk preferences can change with context. The central problem with this perspective is that noise in observed behaviour is often conceptualized as being completely independent from the decision-making processes that guide choice. This stands in stark contrast to many findings within the field of perceptual decision neuroscience showing that the amount of randomness in observed decisions is usually tightly linked to the amount of bias in perception[33–39].

Based on this rich body of work in perceptual neuroscience, we argue here that (at least parts of the) contextual variability and stochasticity in revealed risk preferences might stem from the neurocognitive perceptual processes that precede subjective valuation. Human decision-makers cannot directly observe the objective variables that should determine their choice (i.e., probabilities and potential payoffs). Rather, they must rely on noisy and biased percepts of these variables, stored in neural representations of the sensory input. Therefore, their decisions should be highly sensitive to how information is presented, in ways that should be predictable based on a mechanistic understanding of the involved perceptual processes[29].

This general idea - that perceptual biases may play a role in economic choice - is by no means new. Seminal theories in behavioural economics and economic psychology have long suggested that human decision-makers decide *as if* their perception of the relevant variables was distorted[4,40–42]. However, these classical models treat these distortions as a given and take no stance on where they come from and what determines their shape and strength. For example, the parameters of prospect theory[4] merely describe the over- and underweighting of probabilities but give no further explanation for their origins. This precludes such theories from explaining, let alone predicting, how different contexts modulate choice.

Notably, this agnostic stance towards perceptual distortions of choice-relevant variables has changed in recent years, with a new wave of models of economic choice attributing classic aspects of risk preferences, such as risk and loss aversion, to noisy and biased perception[43–46]. Crucially, these models incorporate theories from psychophysics to describe decisions as a fully rational solution to an optimisation problem that is based on inherently noisy representations of the choice-relevant information. To take optimal choices, our brain makes the best of these noisy signals by applying principles of Bayesian inference[37,47] and/or efficient coding[39,48], which can lead to biases in individual percepts but

is nevertheless beneficial because it reduces the average error in payoff estimation. For example, there is a well-known positive correlation between noise levels and central tendency (CT) bias[49]: With increased noise, participants tend to regress their percepts of stimulus values towards the mean value of earlier observed stimuli. The Bayesian interpretation of this is that participants increasingly revert to their prior beliefs about possible stimulus values when noise gets larger[29,37]. This CT bias might explain substantial parts of risk aversion[43]: Risk-averse individuals might not actually have concave utility functions but may in fact try to maximize expected values. However, they simply perceive the larger monetary amounts that come with risky prospects as less substantial than they actually are (and vice versa for safe prospects).

We have recently provided initial neuroscientific evidence for this claim, by showing that there is a strong link between the noisiness of people's neurocognitive magnitude representations in parietal cortex during perceptual judgments and the amount of risk aversion people exhibit in separate economic choices[50]. This initial demonstration now makes it possible to address important questions about the neurocognitive origins of risk preferences. First, what determines whether individuals show categorically distinct risk preferences such as risk-seeking, risk-neutral, and risk-averse behaviour[5]? These categories currently still largely elude perceptual models of risky choice[43,46]. Second, preferences appear highly sensitive to contexts: Choices can differ substantially depending on how decision problems are framed[4], such as in which order options are presented[28] or which choice options were seen in earlier choice problems[27]. Can we mechanistically account for the influence of context on economic choice, by studying how they alter the perception of the choice-relevant information? Finally, as alluded to above, economic choice behaviour is profoundly variable even without any changes in context[7,29,30]. Where do these apparent fluctuations in risk preferences come from? Can they originate from endogenous fluctuations of neural noise, in analogy to how such fluctuations affect perceptual decisions about low-level visual features[51]?

To address these questions, we introduce a general computational model of choice, the *Perception and Memory-based Choice Model (PMCM)*. The model builds on the assumptions of earlier perceptual models of risky choice[43,50] in that it frames risky choice as a Bayesian inference process on noisy percepts of potential payoffs. However, in the PMCM, the noisiness of the different percepts relevant to the choice is no longer static but depends on the particular context of a specific trial. Specifically, in the experiment

presented here, the noisiness of the representation of a choice option may depend on both whether a choice option is perceived directly or held in working memory and on the acuity of neural processing on a particular trial. Thus, the PMCM makes it possible to characterize the psychological and neural mechanisms by which both exogenous environmental contexts and endogenous (physiological) factors can shape economic choice on a moment-to-moment basis. This enables us to provide a decisive test of perceptual theories of risky-choice mechanisms using biological data.

In the following, we will first describe the risky choice paradigm we developed to modulate the fidelity with which choice options are represented in the brain, by manipulating the order in which they are presented. Furthermore, the paradigm allows us to extract an fMRI signal that corresponds specifically to the acuity of the perception of the payoff of the first choice option, independent from any choice-related neural activity that comes later in the trial[50]. We will then introduce in detail the PMCM and show how it can explain why some people are generally risk-seeking and some are risk-averse, as well as why people appear risk-averse for some sets of choices but risk-seeking for others. Finally, we will show that random fluctuations of sensory neural noise - the acuity of neural magnitude representations in the right intraparietal cortex as measured using inverted encoding models[50,52,53] - relate mechanistically to choice consistency and risk preferences in tandem, in line with a Bayesian perceptual account of risky choice. Our results provide conclusive evidence that risk preferences and their variability across trials and contexts originate (at least partially) from aspects of perceptual neural processing in parietal cortex. These links can be captured by a novel Bayesian perceptual model of risky choice that can explain the observed data mechanistically, as opposed to classical models based on expected utility. This has profound implications for economic, psychological, and neuroscience theories of risk-taking, as well as the experimental paradigms used to study and evaluate risk attitudes in theoretical and applied contexts.

Results

Experimental paradigm

Thirty participants (14 female, aged 20-34) performed the task twice: Once in a 3 Tesla (T) scanner and once in a 7T scanner. To study how risk preferences relate to the acuity of perception and the underlying neural representations, we developed a new experimental

paradigm based on our earlier work[50]. In our paradigm, participants had to choose between a sure payoff and gamble with a 55% probability of winning a larger payoff (Fig. 1a). Crucially, the payoffs of the safe and risky options were presented sequentially as clouds of 1-Swiss Franc coins, preceded by a piechart indicating whether the probability of a payoff was 55% or 100%. Thus, options were presented either earlier or later in time, regardless of their riskiness. This design aimed to increase working memory noise for the first-presented option, thereby enhancing CT biases for the first-presented option.

The payoffs were presented as coin clouds (rather than Arabic numerals) because we know that such stimulus numerosities can reliably be decoded from rIPS[50,54]. However, note that we have recently shown that decisions based on symbolic (i.e., Arabic numerals) and non-symbolic (i.e., coin clouds) presentations of magnitudes are psychometrically very similar and rely on the same approximate number system[50].

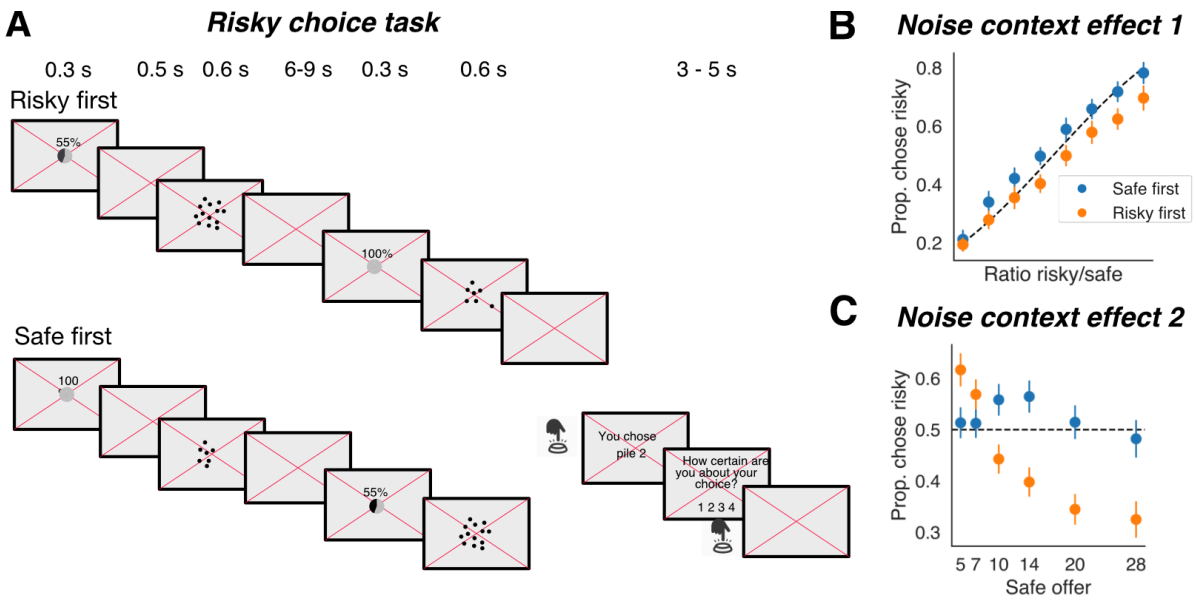

Figure 1: A) *Participants were incentivized to choose between two prospects: A risky option with 55% probability of receiving the payoff and a safe option with 100% probability of receiving the payoff. Prospects were presented sequentially (6 to 9 seconds in between) as clouds of 1-CHF coins, and payoff probabilities were presented as both piecharts and symbolic percentages just before the payoff information. Crucially, either the risky or the safe option was presented first and thus had to be held in working memory (all choice sets occurred twice for every order for every session).* ***B)*** *Average choice behaviour confirms that participants were more likely to choose the risky option when the safe option was presented first, in line with that assumption that options*

presented first (last) are noisier (less noisy) and thus more prone to a central tendency effect. Error bars correspond to the standard error of the mean over participants. ***C)*** *The probability that participants chose the risky option depended on the absolute magnitudes of the choice options, particularly when the risky option came first. This is a clear example of a preference reversal: For relatively small-stakes gambles, participants become (more) risk-seeking when the risky option is presented first. Conversely, for relatively large-stake gambles, they become more risk-averse.*

Different noise contexts shift risk preferences, as predicted by Bayesian inference on noisy payoff representations

We first examined how exogenous factors that modulate neurocognitive noise – in our case, the presentation order of the options – impacted choice behaviour. Psychophysical work on the noisiness of working memory[55–57] suggests that the neurocognitive representation of the initially presented payoffs, retained in working memory, are subject to more noise compared to the options presented subsequently. Thus, taking a perceptual Bayesian perspective[29,37,43,50], we predicted that those options that were presented first should be more sensitive to the central tendency (CT) bias, resulting in overestimation of relatively small payoffs and underestimation of relatively large payoffs. As a consequence, when a relatively small risky payoff was presented first, participants should be more likely to choose it compared to when it was presented second. Conversely, when a relatively large risky option was presented first, it should be less likely to be chosen. For safe options that were presented first, we expected an analogous pattern - in other words, elicited risk preferences should be categorically changed by presentation order and overall stake size.

Analysis of the data confirmed these predictions: We found both an order effect (Fig/ 1B; 3T: $F(1, 29) = 14.49$, $p<0.001$; 7T: $F(1,29) = 5.83$, $p<0.001$) and a main effect of the absolute stake size (defined as the magnitude of the safe option; Fig. 1C; 3T: $F(5, 145) = 6.15$, $p<0.001$; 7T: $F(5, 145) = 5.88$; $p<0.001$), but crucially also the predicted interaction effect between order and magnitude (Figure 1C; $F(5, 145) = 14.21$, $p<0.001$; 7T: $F(5, 145) = 13.45$, $p<0.001$). Indeed, when the risky option came first, participants became risk-seeking and were more likely to choose the risky option when it was relatively small, but they became risk-averse and chose the risky option less when it was larger. This is consistent with the predicted CT bias towards the centre of the range of plausible values in the experiment (see Fig. 2A for a graphical illustration).

The Perception and Memory-based Choice (PMC) Model

To account for more complex risky choice environments, like the one in our experiment, we developed a novel perceptual model of (risky) choice. The crucial new feature compared to the models employed in earlier work[43,50] is that the fidelity with which different choice options are represented can dynamically change as a function of exogenous or endogenous context. For example, in our particular experiment, the perception of the first- and second-presented payoffs can be differentially precise, as the noisiness of the neurocognitive payoff representation kept in working memory can be expected to be higher than the representation of the currently perceived payoff[57]. A second novelty of our model is that it allows for different prior expectations about specific choice options based on secondary cues. For example, in most risky choice experiments, the payoffs of risky options are, on average, substantially higher than those of safe options, and the sequential cued presentation of the options makes it possible for participants to use this information to their benefit. Note that both these features of our model and experiment resemble real-life choice situations, where options are rarely perceived exactly simultaneously and are most often considered sequentially. By explicitly accounting for this in our design and model, we could test whether and how participants' decisions are affected by this feature of a typical choice situation.

The full PMC model we employed in this study has six parameters: (1) the noisiness with which the first option is perceived (ν_1), (2) the noisiness with which the second option is perceived (ν_2), (3) the mean of the prior on risky payoffs (μ_x), (4) the mean of the prior for the safe payoffs (μ_c), (5) the standard deviation of the prior on risky payoffs (σ_x), and (6) the standard deviation of the prior on safe payoffs (σ_c). Note that these six parameters can be estimated in our particular experimental paradigm because the noise of the evidence is experimentally manipulated by order, orthogonal to the riskiness of the option. We confirmed the recoverability of the parameters of our model using multiple strategies. When the model was fitted separately to the same participants' data for the two scanner sessions, the six parameter all correlated across the two sessions, with correlation coefficients r(29) between 0.41 and 0.76 (all $p<0.05$). A parameter recovery study using the estimated parameters as generating parameters showed substantial correlations between generating and recovered parameters, ranging from 0.74 to 0.93. See Supplementary Text 1 for more details.

Posterior predictive plots show that our model does an excellent job at predicting the observed empirical patterns at the group level, including the interaction between magnitudes and order of presentation (Fig. 2B). Moreover, our model also explains highly divergent behaviour across individual participants: Some participants are not influenced by order and/or overall stake sizes, and some participants are risk-seeking rather than risk-averse. Supplementary Fig. 1 gives some examples of typical behavioural patterns of representative participants and their posterior predictive plots.

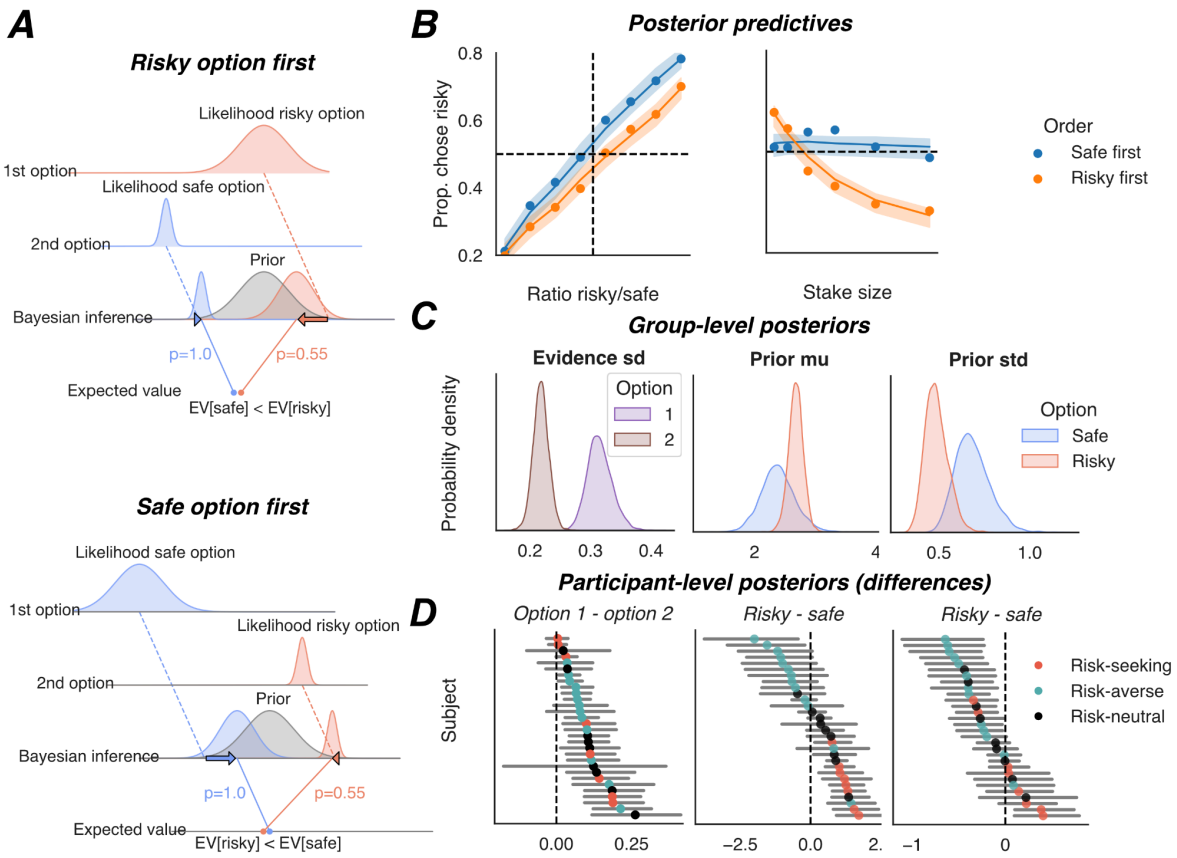

Figure 2: A) *Illustration of the intuition behind the Perception and Memory-based Choice Model (PMCM): When an option is presented first, its evidence will be noisier because the option needs to be held in working memory and the participants has no direct access to the corresponding stimulus during the decision (unlike the second option). The first option will therefore be more influenced by the prior than the second option and have a larger CT bias. Presentation order can therefore lead to preference reversals.* ***B)*** *The posterior predictions of the PMCM (95% credible interval as shaded area) can account for the empirically-observed effects (data points as markers), in contrast to alternative models (See Figure 3).* ***C)*** *The estimated group parameter posteriors of the extended model suggest that the payoff of the first option is encoded with substantially more noise*

than the second option (left panel). Furthermore, the prior for risky options is estimated to have a higher mean payoff (middle panel; although this difference is significant only for some participants) but also a more narrow range (right panel). Thus, risky payoffs are more prone to regression effects than safe payoffs. ***D)*** *Participant-wise estimates of the differences between key parameters in the model, i.e., between options presented first/second and the safe versus risky prior. Dots are mean estimates and lines are 95% credible intervals. Almost all participants have significantly ($p_{Bayesian} < 0.05$) more noisy evidence about the first-presented payoff (leftmost panel), but only a subgroup employs different priors for risky and safe options (middle/right panel). This mean difference in risky and safe priors relates to the apparent risk preference of the participants (i.e., Risk-seeking/risk-averse or risk neutral). For this figure, data from the 3T and 7T sessions were combined; see Supplementary Fig. 2 for separate analyses of the two sessions.*

The first key goal of our study was to explain how seemingly categorically different risk attitudes (e.g., risk aversion and seeking) may emerge from noisy perceptual inference processes. Our data reveal that there is indeed considerable variability across both participants and choice contexts when it comes to whether behaviour is 'risk-seeking', 'risk-neutral', or 'risk-averse'. Indeed, we found that under some circumstances, our experimental population was risk-seeking on average, namely when the risky option was presented first, and the safe option was relatively small (5 or 7; Fig. 1C). Our model-based inference that participants are particularly noisy and/or optimistic about potential prospects now characterizes the latent decision mechanisms and how they mechanistically lead to seemingly different behaviour in specific contexts. This appears more useful than a purely descriptive categorization based on average elicited preference.

The second main goal of our study was to explain why preferences can shift across different contexts. Our model can naturally explain such context-specific preferences: The risky payoff is particularly overestimated when it is relatively small and noisy. Moreover, it is well-known that a non-negligible fraction of experimental populations shows risk-seeking behaviour on average[5,58]. Current perceptual models of risky choice cannot account for this without assuming additional distortions in probabilities[43,46]. In contrast, our model can: Risk-seeking participants have particularly optimistic prior beliefs about risky payoffs and are particularly risk-seeking when their percepts of the objective risky payoff are noisier (see Fig. 2D; left and middle panel).

One question about our model might be whether it is unnecessarily complex, as it contains many parameters to fit the data. We addressed this question with both qualitative predictive checks and quantitative model comparison techniques, testing whether both dynamic noise and different priors for risky/safe options are strictly necessary to explain the empirical data[59,60]. To do so, we compared the PMCM to four simpler models. The first model was a baseline model where the noisiness of the first and second options were identical and the priors were the same for risky and safe options (model A[43,50]). In the second model, the noisiness of the first and second options was constant, but the priors for risky and safe options could be different (model B). In the third model, the noisiness of the first and second options could be different but the priors for the risky and safe options was shared (model C). Finally, we also compared our models to a standard expected utility model (Model D[4,23]). The posterior predictive plots are presented in Figure 3. Visually, it is evident that none of the alternative models can explain the interaction effect of magnitude and order on the proportion of risky choices. Moreover, a formal model comparison using the Expected Posterior Log Density[60] shows that the PMCM is vastly superior to the other four models. The difference in ELPDs is at least 21 standard errors (Figure 3E). When we used model stacking[61], the model weight of the PMCM was over 95%. These measures thus provide evidence for both mechanisms (i.e., varying noise for order and varying priors for risikness) incorporated in our model. To make sure that our model comparison approach was sufficiently powerful, we also simulated 100 data sets using the 5 different models and used the same technique to estimate which was the generating model. When the PMCM was the generating model, it was correctly identified 100/100 times (See Supplementary Text 2 for more details), demonstrating that our model makes counterintuitive qualitative predictions that are fully in line with empirical data and can only be captured by this particular model and not the alternatives.

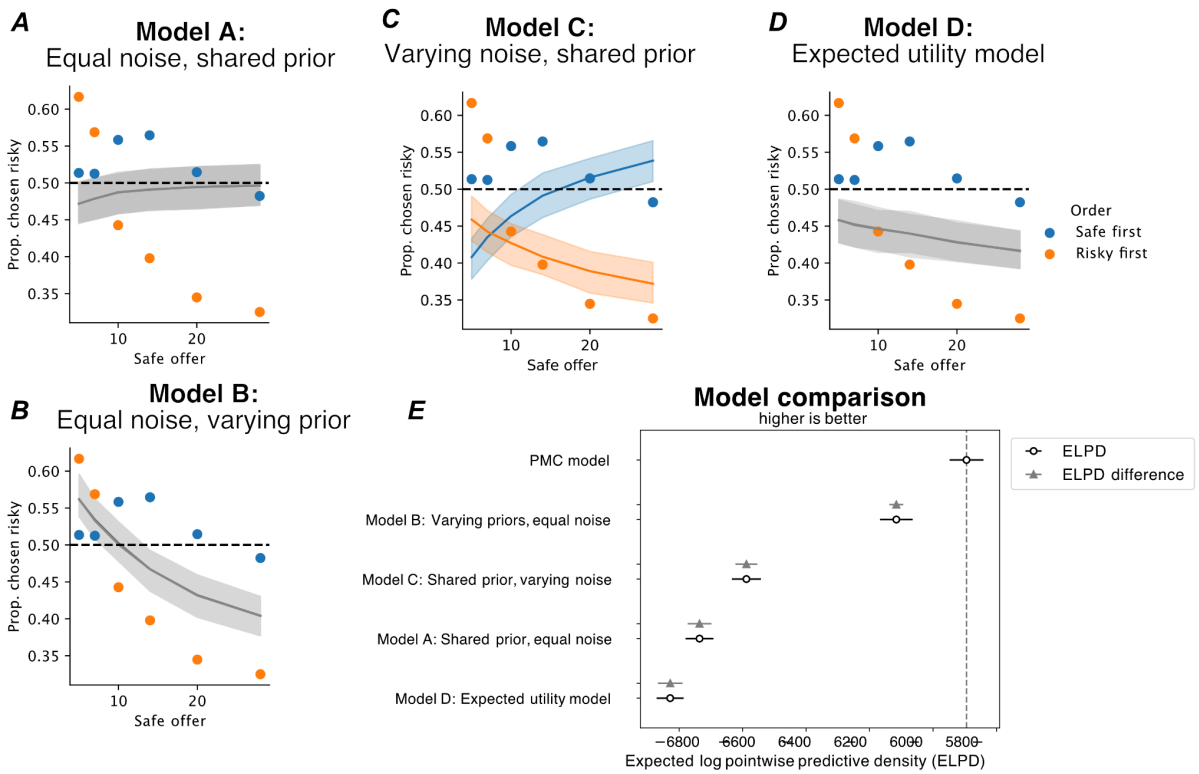

Figure 3: A-D) *Posterior predictive plots for alternative models of different complexity. Unlike the PMCM, none of the tested models can explain all qualitative patterns in the data. Compare to Figure 2B.* ***E)*** *For formal model comparison, we used expected log-predictive density (ELPD), which estimates the likelihood of unseen data given the model parameters, making it an effective measure of out-of-sample performance[60]. As a state-of-the-art model comparison technique, ELPD comparison demonstrates that the PMC model significantly outperforms the other models tested (error bars are standard errors on the ELPD).*

Finally, posterior estimates for the group mean of the model parameters (Fig. 2C) reveal that, as expected, participants have noisier payoff representations for first-presented versus the second-presented option ($p < 0.001$ for both sessions). Notably, while at the group level, the subjective prior for risky payoffs does not have a higher mean than the prior for safe payoffs (3T: $p_{Bayesian}$ =0.16, 7T: $p_{Bayesian}$=0.37, both: $p_{Bayesian}$ =0.16), there were 13 participants who had a higher mean prior for risky than safe options (95% credible interval of the difference does not overlap with 0, see Fig. 2D). These individual parameter estimates suggest that some participants take into account that risky payoffs are higher on average whereas others do not.

In sum, our novel experimental paradigm and the PMCM can mechanistically characterize how a common and relevant context effect (whether options are held in working memory or perceived immediately) impacts the apparent risk preference of the participants. The model can explain why the experimental population is risk-averse in some contexts but risk-seeking in others, and it can account for individual differences in risk preferences.

Decoded payoff representations in parietal cortex predict noisiness and bias in choice

Having established that individual risk preferences and changes in preference across different choice contexts can be explained by our Bayesian perceptual account of risky choice, we now addressed the final question of our study: Where do the trial-to-trial fluctuations in risk preferences come from? We hypothesized that some choice variability – over and above the variability determined by context and individual differences – can be explained by momentary fluctuations in the fidelity of neural representations[62–65]. Our previous work has shown that individual differences in the precision of parietal magnitude coding are predictive of individual differences in risky choice behaviour: Participants with noisier payoff magnitude representations tend to resort more to their prior beliefs and are, on average, more risk-averse[50]. This paves the way for the question whether there is a comparable relationship between neural noise and behaviour *within* single decision-makers. Such a relation could in principle be expected based on findings in perceptual neuroscience: For examples, trial-to-trial fluctuations in judgments about the orientation of Gabor patches are predicted by fluctuations in orientation representation in primary visual cortex[52,53,66], and judgments about movement directions relate to differences in neural activity in middle temporal area (MT)[67,68].

To be able to test this hypothesis, we first fitted a numerical receptive field (nPRF) model[50,54] to single-trial BOLD responses locked to the *first payoff* presentation, to preclude that any decision-related activity would contaminate our measures of neurocognitive representation (Fig. 1A). The nPRF model assumes that patches of cortex are tuned to numerosity - i.e., they have a preferred magnitude to which BOLD responses are largest - and that the size of the response to a stimulus decreases exponentially with its logarithmic distance to the preferred numerosity. Numerically tuned cortical areas were similar to previous studies: The surface-based locations where the model predicted single trial responses best (high explained variance, R^2) largely followed the parietal mask based on our earlier study[50] (see

Fig. 4A). Moreover, within the mask, vertex-wise R^2 values highly significantly correlated across the 3T and 7T fMRI sessions within participants with, on average, r = 0.25 (t(29) = 6.2, p<0.001) and preferred numerosities with r = 0.15 (t(29) = 6.0, p<0.001). These results confirm that the intraparietal sulcus contains participant-specific patterns of numerosity encoding that generalize across sessions and even MRI scanners.

After successfully fitting the nPRF model, we used a Bayesian inversion scheme to decode posterior estimates of presented numerosities from unseen fMRI data (leave-one-run-out cross-validation)[50]. Note that this method yields the posterior distributions over numerosity given the empirically observed single-trial brain activity pattern. Thus, the analysis does not only give us a point estimate of the expected numerosity (mean of the posterior) but, crucially, also a measure of the uncertainty surrounding that point estimate. Earlier work in perceptual neuroscience has shown that the posterior uncertainty surrounding a stimulus feature decoded from brain activity predicts the randomness and bias of choices and judgments on those very stimulus features[50,52,53].

Before linking neural uncertainty to behaviour, we first assessed the fidelity of the decoder. The presented payoff magnitudes were decoded well above chance on the level of single trials, with an average correlation between actual numerosity and decoded numerosity of r=0.176 (3T; t(29) = 7.1; p<0.001) and r=0.16 (7T; t(29) = 8.0, p<0.001; see also Fig. 4B). Importantly, the decoded neural uncertainty (s.d. of the decoded posterior) was significantly correlated with the error of the decoder (absolute difference between mean posterior and actual numerosity) with r=0.33 (3T; t(29)=9.8, p<0.001) and r=0.38 (7T; t(29)=18.8, p<0.001). Since the uncertainty of the decoder relates directly to how well it can actually decode a given neural pattern, we can be confident that the variance in the decoded posteriors is meaningful and a useful proxy for the neural noisiness of the payoff magnitude representations that the decision-makers base their choices on[50,52,53].

We also conceptually replicated an important result reported before by ourselves[50] and others[69], namely that participants with particularly noisy neural representations of magnitudes in the right parietal cortex also show more noisy and biased behaviour. Specifically, participants who had a higher correlation between neurally decoded numerosities and the presented numerosities tended to have a less noisy representation of the first stimulus magnitude according to our behavioural PMCM (the correlation between decoding correlation and the dispersion of the likelihood of the first option v_1, r(29) =-0.48, p =0.007 for 3T and r(29) = -0.42, p=0.021 for 7T). Importantly, participants for which we

decoded posteriors with, on average, a higher standard deviation also had a larger v_1 -parameter according to the PMCM (r(29) = 0.44, p=0.014 for 3T and r(29) = 0.38, p=0.039 in the 7T data), thus replicating our earlier findings[50] twice, on different scanners.

After reconfirming with these replications both the robustness of our IPS-signal decoder and the relevance of these parietal regions for individual risk preferences, we proceeded to test whether *within each participant*, trial-to-trial fluctuations in apparent risk preference are related to latent fluctuations in the neural code that represents the potential payoffs that are at stake. To test this hypothesis carefully, we first further refined it into two subhypotheses: On trials where neural payoff representations are particularly noisy, choice behaviour should (a) become less consistent and (b) more biased towards prior beliefs. In the PMCM, both effects can jointly be explained by an increase in noise. However, we aimed to first test both hypotheses separately. To do so, we used a standard psychometric model that fits a psychometric curve with both an indifference point and a psychometric slope to the choice data as a function of the log-ratio of the risky and safe payoffs[43,50]. To make sure we found an effect of neural uncertainty over and above any order- and magnitude-effects, we performed a median split separately for every possible first-presented payoff and fitted seperate psychometric curves to these two sets of trials that were matched in payoffs and order but showed relatively high or low neural noise.

In line with our expectations, the psychometric slope was substantially more shallow for trials with a higher decoded neural uncertainty ($p_{Bayesian}$=0.003; $p_{Bayesian}$=0.0458 for the 3T data set; $p_{Bayesian}$=0.0238 for the 7T data set). Thus, the more noisy the signal was according to our neural decoder, the more randomly (i.e., independent from the presented payoffs) participants chose between the options. To test whether participants were more biased in their perception of the potential payoffs when their neural representations were particularly noisy, we tested whether estimated indifference points were further away from risk-neutrality when neural noise was higher. To do so, we used the *risk-neutral probability* (RNP), which defines the indifference point as the probability that an experimenter would have to present to a perfectly risk-neutral (expected value-optimising) participants to be indifferent about a choice. In our paradigm, a RNP of 55% corresponds to risk neutrality, a RNP below 55% corresponds to risk aversion, and an RNP above 55% to risk-seeking. When we fitted a hierarchical Bayesian psychometric model and sampled the resulting participants-, payoff- and order-specific RNPs. These RNPs were indeed farther away from risk-neutrality (55%) when the neural uncertainty was higher (18.5 percent points, s.d. 9.2

versus 16.7 percent point, s.d. 9.2; $p_{Bayesian}$<0.001, Fig. 4C; these results replicate when separately estimated for two sessions, $p_{Bayesian}$= 0.012 for 3T and $p_{Bayesian}$= 0.013 for 7T). Thus, the less precise the numerosity-tuned responses in IPS according to our decoder, the more participants reverted to their prior beliefs and the less risk-neutral they became in their preferences.

Finally, as the ultimate test of the hypothesis that trial-to-trial fluctuations in risk preference are (partly) driven by fluctuations in neural noise, we tested whether an increase in the noise parameter of the PMCM can explain the observed link between neural acuity and behavioural consistency and choice. We hypothesized that, in terms of PMCM parameters, the first choice option should be represented more noisily when the corresponding decoded signal was less precise. Therefore, we refitted the PMCM to behavioural data, but now all six model parameters were estimated as a linear sum of a (participants-wise) intercept and a regression parameter that was multiplied with the z-scored trialwise neural uncertainty measures (i.e., the standard deviation of the decoded posterior). If this latter regression parameter differed from 0, the corresponding latent variable linearly varied with neural uncertainty[70,71]. This analysis confirmed that both the noisiness of the first option (3T: $p_{Bayesian}$ =0.02; 7T: $p_{Bayesian}$ =0.04; both: $p_{Bayesian}$ =0.009; See Fig. 4 and Supplementary Fig. 3) and the standard deviation of the prior on safe payoffs (3T: $p_{Bayesian}$ =0.02, 7T, $p_{Bayesian}$ =0.01; both: $p_{Bayesian}$ =0.004; See Fig. 4 and Supplementary Fig. 3) linearly increased with increased neural uncertainty. These results align with the psychometric modelling results: When neural noise is high, the representation of the payoff of the first option becomes noisier, resulting in larger CT biases and more variable behaviour. However, the increased dispersion of the prior belief about safe payoff magnitudes with increased uncertainty reveals that it is mostly the risky (rather than safe) options that drive the increased CT bias with increased neural uncertainty.

In conclusion, we successfully decoded payoff magnitude representations during economic choice from right parietal cortex, replicated earlier findings of a direct link between the acuity of an individual's numerical magnitude representation in the IPS and their choice consistency and elicited preferences, and, crucially, find that trial-to-trial fluctuations in the acuity of payoff representations in parietal cortex are mechanistically linked to trial-to-trial fluctuations in choice consistency and risk preference. This provides direct biological

evidence that the endogenously fluctuating precision of neural magnitude representations underlies time-variations in revealed risk preferences.

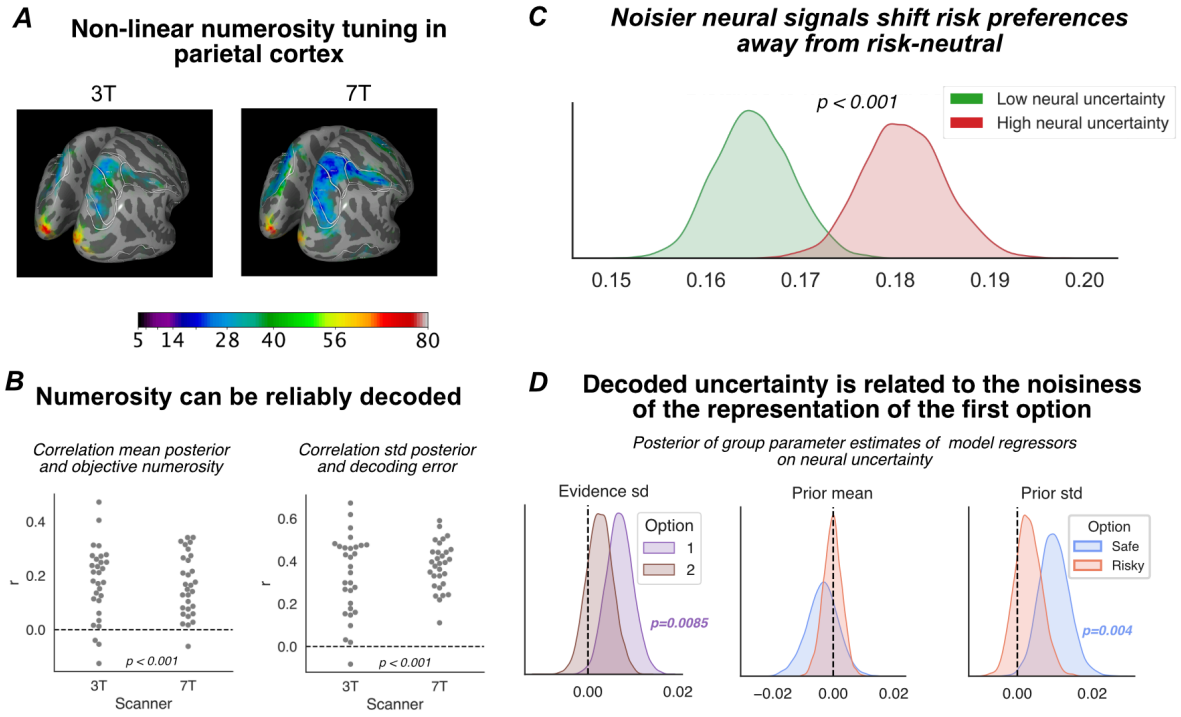

Figure 4: A) *Numerical population receptive field (nPRF)-mapping reveals non-linearly tuned numerosity-sensitive BOLD responses around the intraparietal sulcus, closely following the ROI drawn on an independent data set (Garcia et al., 2022). Here we show the average preferred numerosity across all participants in fsaverage-space.* ***B)*** *Almost all participants (27 out 30 for 3T, 29 out 30 for 7T) show a positive correlation between the presented stimulus numerosities and decoded posterior means for single trials from out-of-sample fMRI data. Trial-to-trial fluctuations in the width of the decoded posterior are indeed predictive of the objective error of the mean posterior.* ***C)*** *Choice behaviour on trials with a higher decoded neural uncertainty tends to be more biased: the RNP is further away from risk neutrality (55%). The panel shows posterior estimates of the average participants-wise distance to risky-neutrality (abs(RNP - .55)). Thus, if participants were already risk-seeking on a particular trial type (particular order and particular safe payoff), they behaved even more risk-seeking when neural noise increased. The opposite effect is observed for participants and trial types for which behaviour was risk-averse.* ***D)*** *When the main six parameters of the PMCM were allowed to vary linearly with trial-to-trial fluctuations in the decoded neural uncertainty, both the noisiness of the representation of the first option and the dispersion of the prior on safe payoffs increase with neural uncertainty decoded from the first payoff stimulus. The*

noisiness of the second option, the location of the priors, and the dispersion of the prior on risky payoffs were not related to neural uncertainty.

Discussion

Risk preferences play a central role in many aspects of our behaviour, but we still don't understand where they come from, why they change across different contexts, and why they can even differ for repetitions of identical choices in the same context. Here, we provide modelling and neurobiological evidence that rapid changes in individual risk preferences can originate in the neurocognitive processes that underlie our perception of (monetary payoff) magnitudes. We introduced a new experimental paradigm that modulates the noisiness with which different choice options are perceived, by presenting them in different orders as in typical everyday choice situations where options are considered one after another. This sequential presentation made choice options more/less prone to working memory noise[56,57], resulting in central tendency effects[37,49] that lead participants to perceive the very same choice options as larger or smaller depending on their presentation order and magnitude. We captured these effects with a new Bayesian model of risky choice - the PMCM - that explicitly accounts for dynamic fluctuations in the noisiness with which different choice options are perceived, as well as for different prior expectations based on the context of a particular choice problem. Crucially, we also used fMRI and inverted encoding models to provide neural evidence for such rapid fluctuations in neurocognitive noise and showed that these predict risky choice in a manner consistent with the PMCM.

Our combined results have profound implications for both theoretical and empirical work on risk preferences. First, in line with other recent work[26,27,30], they defy the conventional economic wisdom that preferences are stable[2] and demonstrate that elicited preferences are systematically unstable, due to fluctuations in the noisiness of neurocognitive representations of the relevant decision variables. This relevance of noise in the decision-making process for elicited risk preferences dovetails with earlier work highlighting that differences in risk preference may easily be conflated with differences in choice consistency[72–74]. However, rather than assuming that noise may affect choices unsystematically at a late stage of the decision process, our model emphasizes that noise originates early in the decision process, during perception of the choice-relevant information, thereby determining risk preferences before any actions are taken that would reveal them.

A second key implication of our study – congruent with other recent work[43,75,76] – is that a large part of inter- and intra-individual variability in risky choice behaviour can be explained by fluctuations in basic perceptual neurocognitive representations, over and above any possible differences in subjective valuation of the choice options. We show that decision-makers can show preference reversals (i.e., become risk-seeking rather than risk-averse) simply due to changes in the order in which choice options are presented. This raises the crucial question to what extent variability in risky choices really reflects subjective valuation (as opposed to noisy perception), as usually assumed in standard economic models. Notably, our PMC model, which contains no subjective valuation process, could explain a wide range of choice patterns across subjects and contexts, whereas a standard economic choice model based exclusively on subjective evaluation (the EU model) failed to do so. While this evidently does not prove that subjective valuation is not involved in risky choices, it still suggests that perception may play a more important role, at least in the small-stake laboratory experiments widely used to study risk preferences.

This substantial impact of perception on elicited preferences (rather than valuation) might explain the 'risk elicitation puzzle': the fact that elicited individual risk preferences are only marginally correlated across elicitation methods[6]. Moreover, the central role of perceptual effects for elicited risk preferences may have profound implications for welfare economics, which often relies on elicited preferences to calibrate models of the impact of economic policies[77]. Thus, future work should attempt to further unravel potentially separate contributions of neurocognitive processes related to subjective valuation versus perception to individual preferences and, if possible, develop economic choice tasks where perception can be dissociated from participant's subjective valuation. For this agenda, it may be important to take seriously the proposed conceptual distinction between elicited risk *preferences* (overt behaviour) and risk *attitudes* (underlying latent traits)[24]; the latter may arguably be a more relevant target variable for welfare-related questions than overt choices alone[77].

Future studies attempting to dissociate valuation and perception should systematically manipulate both sets of processes. Valuation may be experimentally manipulated by changing objective choice properties and comparing qualitatively different decision-makers, while perception may be influenced by orthogonally manipulating the fidelity of the choice-relevant information. Here we did so by representing potential payoffs with non-symbolic stimulus arrays and changing their order. One might argue that this choice

context may induce effects in a purely 'low-level perceptual' manner that should be absent for choices with more common Arabic numerals. However, there is ample evidence that Arabic numerals are far from immune to perceptual effects[78]. For example, when participants have to make decisions about rapidly-presented Arabic numerals, they are sensitive to order effects[79] and the underlying statistics of the presented numerals[80], just as for the non-symbolic presentation formats in the study presented here. Furthermore, recent neuroscience studies have shown that numerosity-tuned regions similarly represent both symbolic Arabic numerals and non-symbolic stimulus arrays[81]. Finally, our recent work[50] has shown that the performance on a perceptual task involving the numerosity of stimulus arrays predicts both choice consistency and risk preference in independent risky choice tasks involving both non-symbolic and Arab numerals. This highlights that non-symbolic and symbolic presentation formats can be combined to manipulate the noisiness of choice information, in order to unravel valuation and perception.

The finding that our Bayesian model of the inference underlying perception could account for several counterintuitive context effects on risk preferences suggests that this type of model may be important to fully understand several other effects documented in the literature. For example, another well-established determinant of the acuity of choice information is the time that choice information is attended to. Indeed, eye-tracking data show that both the order and duration with which participants attend to relevant choice variables profoundly influence economic choice[82]. Importantly, participants act *as if* they multiply relative values of choice options with the amount of time they gaze upon a choice option[83,84]. This multiplicative effect is fully consistent with a Bayesian account where attention increases the fidelity with which we perceive information. Thus, particularly valuable options are chosen more often with increased attention, but less-valuable options less often (since the CT effect will decrease as a function of dwell time). Future studies should thus attempt to explicitly link such models to the type of Bayesian models of perception we employed here. Another way in which perceptual processes preceding putative valuation may affect preferences are changes in the statistics of the local environment[85]. Indeed, it is well-known that elicited preferences are sensitive to the larger choice set across an experiment[27]. Future studies should thus attempt to further test with rigorous Bayesian modelling whether these choice set effects are not only qualitatively but also quantitatively consistent with a model where subjective priors adapt to the local choice context[37,46,86].

Our work also has implications for existing neuroeconomic studies and opens up some exciting new research directions. First, studies attempting to identify neural correlates of subjective value[87] need to take into account that at least under some conditions, subjective values inferred from choice behaviour might be a compound measure that also includes perceptual noise and biases, which can profoundly influence any decision variable constructed from this information. This means that neural correlates of subjective value might include perceptual areas as well as 'true' valuation areas[88,89]. However, our work also suggests that computational modelling of behavioural and neural data could help decompose these sources of choice variability[90]. It will be interesting to see whether explicitly incorporating perception in such models can help to elucidate whether subjective value is represented in the brain completely independently from perceptual variables.

Second, our results suggest a key role for parietal regions in economic decisions that involve (numerical) magnitudes. Most neuroeconomic theories propose that, during choice, subjective values are represented in the ventromedial and/or orbitofrontal cortex (vmPFC/OFC)[91], whereas parietal cortex is generally conceptualized as a brain region that integrates the final evidence for different choice options based on subjective or objective stimulus properties[92–94]. However, our results suggest that, at least when magnitudes are involved, parietal cortex also directly represents initially choice-relevant stimulus information during perception of the choice problem. This provides a new explanation for earlier discoveries of neural substrates of subjective value of specific choice options in the parietal cortex of non-human primates[95,96], as well as recent work using brain stimulation that shows that activity in parietal cortex is causally involved in risky choice[97,98].

Clearly, the precise role of parietal cortex in economic choice remains to be fully elucidated and is likely to be dependent on the specifics of the choice task, as well as the phase of decision-making during which one monitors parietal activity. However, one promising working hypothesis could be that when objective magnitudes are involved, parietal cortex can both represent relevant magnitudes (e.g., probability of payoff[99] or monetary amounts[50]) of the option currently under consideration/attention[99,100], as well as accumulate finaly evidence for choice options, as also found in recent work on perception[101]. Notably, almost all work in (human) neuroeconomics has assumed linear coding of subjective value in large cortical locations that adhere to macro-anatomy (i.e., MNI space). However, our work suggests a non-linear code that is only loosely related to macro-anatomy – at least for parietal representations of potential payoffs (see also work on non-linear coding of

probabilities[99]). More sophisticated fMRI analysis approaches may thus be needed to fully delineate representations of objective stimulus information and subjective values during economic choices[89]. For instance, studies decomposing subjective value in its constituent parts (basic perceptual and subjective) should aim to use analysis frameworks that allow for non-linear codes and take into account individual functional neuroanatomy. An exciting open question for such work may be how fluctuations in early perceptual representations of a choice problem (e.g., potential payoff) covary with prefrontal representations of subjective value.

Our work aligns with a recent body of research that conceptualizes economic choices as rational responses to cognitive capacity constraints[29,38,75,102,103] and makes three new contributions to this literature. First, we present a computational model that can be used to estimate how choice contexts modulate both prior beliefs and perceptual noise associated with different choice options. Second, our PMC model can mechanistically explain how discrete categories of risk preferences (i.e., risk-averse, risk-neutral, risk-seeking) can be understood as a continuum emerging from the interplay between subjective beliefs about potential payoffs and noisiness of perception, and can predict corresponding preference changes across different contexts. Third, we present neuroimaging evidence that fully endogenous fluctuations in the noisiness of *neural* representations of economic variables[23] determine economic preference in line with a Bayesian perceptual account. This last finding also highlights the promise of using advanced neuroimaging data and analysis methods to help validate and refine computational models of economic choice[104]. Future work in this direction may, for examples, link economic preferences to the noisiness of neural representations of other relevant economic choice variables, like probability[75,99,105], time[106,107], and social constellations[17,108].

Finally, our results also have potential clinical and policy implications. First, the abundant preference for gambling has long been a puzzle for economists[109,110]. Might the preference for gambling be explained as a misperception of the potential payoffs? One relevant finding in problematic gambling is increased arousal during gambling situations[111,112], which is known to interact with perceptual biases[113]. Indeed, gamblers report unrealistically optimistic beliefs about potential outcomes[114–116]. Future work might investigate false beliefs in problematic gamblers using explicit Bayesian models of risk perception[117,118]. Such false beliefs might have important policy and moral implications for the public communication about gambling. Our results also have implications for the domain of finance. In personal

banking, it has become common practice to elicit risk preferences when taking on new clients[119]. If perceptual effects partly drive such elicited preferences, these estimations might be erroneous and clients might be offered an investment portfolio that is overly defensive, just because they have relatively noisy numerical perception or overly pessimistic beliefs about potential long-term stock returns.

To conclude, our work reveals that perceptual biases to presentation order and relative magnitudes, as well as brain state, can profoundly impact an individual's elicited risk preferences, and they introduce an experimental and modelling approach that can be used to systematically investigate such effects for a whole range of economic choices. Our findings empirically substantiate emerging proposals that economic preferences should be understood as the fluctuating output of a capacity-limited brain rather than fixed as-is economic preferences[29,38,43,102,103]. Our new model and experimental approach is highly relevant to (neuro)economic research because it formalizes why there might be no such thing as an 'objective' risk preference that is completely independent of context and brain state[6,120], and allows researchers to quantify the corresponding effects. More generally, our study demonstrates that attempts to quantify preferences need to consider the substantial variability in responses and should be mindful of potential confounds like presentation (or fixation) order and the general range of options offered during an experiment. These considerations can profoundly impact real-world practice as well, for example when risk elicitation paradigms are increasingly used to compile investment portfolios[119] or characterize the symptoms of psychiatric disorders[121,122].

Methods

Participants and ethics

Thirty right-handed participants (14 females, ages 20 to 34) volunteered to participate in this study. We informed them about the study's objectives, the equipment used in the experiment, the data recorded and obtained from them, the tasks involved, and their expected payoffs. We also screened participants for MR compatibility prior to their participation in the study. No participant had indications of psychiatric or neurological disorders or needed visual correction. Our experiments conformed to the Declaration of Helsinki, and our protocol was approved by the Canton of Zurich's Ethics Committee.

Procedure

Participants were invited for a total of 4 sessions. Two sessions took place at the 3T scanner and two sessions took place at the 7T scanner (see 'MRI parameters' for more information on scanner type and scanning parameters). Participants always first performed two sessions at one scanner, before the other two at the other scanner. Seventeen (17) participants performed the first two sessions at the 7T scanner, the other 13 at the 3T scanner. During the first and third session –so both at the 3T and 7T scanner– participants performed a calibration version of the risky choice task so we could estimate their average risk preference and choice consistency within a specific scanner environment before they performed the main task of interest. The calibration task was done in the scanner while undergoing anatomical scans. Participants made choices about 96 possible risky gambles (the safe payoff was either 5, 7, 10, 14, 20, or 28; the risky option was a $2^{h/4}$ times the safe option with h being all integers between 1 and 8). These offers were presented twice, once with the safe option first and once with the risky option first. A psychometric probit model with "chose risky option" as the dependent variable and an intercept and the log-ratio of the risky and safe option [43] as independent variables was fitted to these calibration data. The fitted model established the precise mapping between risky/safe payoff ratios and the proportion of risky choices. We then made a participants-tailored design with 8 fractions equally spaced in log-space that –according to the psychometric model– were predicted (equally-spaced) proportions of risky choices between 20% and 80%. These 8 fractions were combined with 6 safe payoffs (5/7/10/14/20/28). Also, all these offers were presented

twice with the safe option first and twice with the risky option presented first (so, for every session, each possible safe/risky/order-permutation occurred twice). This amounted to 192 trials per session. After the anatomical scans and the calibration task, participants performed a numerosity mapper task following Harvey et al. (2013; data not shown in this paper).

For the second session in a scanner, participants filled in all information and consent forms and then immediately performed 192 trials of the risk task in the scanner, spread out over 8 blocks of approximately 5 minutes each.

After all 4 sessions, we selected a random risky choice trial from each of the two calibration sessions and one of each of the main task sessions. For the risky trials, a digital random number generator was used to hand out the risky option 55% of the time. The participants got the average payout across the 4 sessions on top of their hourly fee (30 CHF per hour; approximately 30-35 USD).

Experimental paradigm

The task of the participants was, for every trial, to choose between a certain amount of money (5/7/10/14/20 or 28 CHF) or a gamble with 55% probability of winning a larger amount of money and a 45% probability of winning nothing at all. The choices were presented by a sequence of tailored stimuli. The general sequence is illustrated in Fig. 1A. The screen always contained a red cross with two diagonal lines to keep fixation near the centre of the screen and to not confound the numerosity of stimuli like a standard fixation cross or point might[54]. The start of a new trial was indicated by the fixation cross turning green for 250 ms. Then, after a pause of 300 ms with just a red fixation cross, a pile chart with a diameter of 1 degree-of-visual-angle (dova) was presented for 300 ms to indicated the probability-of-payout for the coming stimulus. This was always either 55% or 100%. Then, after another 500 ms of just fixation cross, a stimulus array of 1-CHF coins appeared that represented the potential payoff of the first choice option. The coins had a radius of 0.3 dova (degrees of visual angle) and were all randomly positioned with their centre within a circular aperture with a diameter of 5.25 dova. The coin stimulus array was presented for 600 ms, after which only the fixation cross was presented for a jittered duration of either 5, 6, 7, or 8 seconds. Then, a piechart indicating the probability of the second payoff was presented for 300 ms, followed by a 300ms fixation screen, and another coin stimulus array, representing the potential payoff of the second option, again for 600 ms. As soon as the

second stimulus array was presented, participants could indicate their response with their index (first-presented option) or middle finger (second-presented option). As soon as they responded, they saw a 1 or 2 indicating which option they had chosen for 500 ms. After the coin stimulus pile was presented, the remaining duration of the trial was either 4, 4.5, 5, or 5.5 seconds. During the time that was left after the feedback stimulus, participants had to indicate "how certain" they were about their choice using a 4-step Likert scale (by pressing response buttons with four fingers, from index finger-pinky). The results from this certainty rating are not presented in this paper.

On the 3T scanner, stimuli were presented using a projector on a white screen at the back of the bore and a hot mirror system on top of the coil system (1920 x 1080). The projector screen was at a distance of 125cm from the participants's eyes and was 42 cm wide, corresponding to a field-of-view of approximately 19 DoVA. At the 7T scanner, stimuli were presented using the Avotec (Avotec, FL, USA) binocular goggle system (800 x 600) with a field-of-view of approximately 25 DoVA.

Behavioural analyses

Psychometric/KLW model

Model specification

Khaw, Li, and Woodford[43] showed that in risky choice paradigms where participants choose between a certain payoff C and a risky payoff X with a probability of payout p, observed choice behaviour can be understood as the outcome of a Bayesian inference process.

Specifically, their model (from on referred to as KLW model) assumes that participants do not make decisions based on the objective payoffs C and X, but based on noisy representations of those payoffs, described as random variables r_x and r_c. The likelihood function describes the probability of noisy representations conditional on C and X:

$$r_x \sim N(log\ X,\ \nu^2),\ r_c \sim N(log\ C,\ \nu^2)$$

As can be seen in the formula, these representations take place in a logarithmically-transformed payoff space. This means that participants will adhere to Weber's law. Thus, in natural space, the randomness of their choice behaviour is predicted by ratios between options rather than absolute differences in natural space. Moreover, the

parameter ν now determines the noisiness of representations and thereby how variable behaviour will ultimately be.

Crucially, the KLW model also assumes that people apply a *common prior* for both the risky and safe options:

$$log\ X,\ log\ C \sim N(\mu,\ \sigma^2)$$

In the KLW model, the μ-parameter has no influence on predicted behaviour. However, because the decision-maker applies the same common prior to both risky and safe options, risky options will always *be relatively underestimated compared to the safe option* (this is because risky options always have higher payoffs than safe options for them to be attractive to the participants). The extent to which underestimation of larger payoffs happens is a function of the ratio between the variance of the likelihood ν^2 and the dispersion of the prior σ^2, β:

$$\beta = \frac{\sigma^2}{\sigma^2 + \nu^2}$$

Specifically, the conditional expected values of the two options conditional on r are:

$$E[X|r] = e^{\alpha+\beta r_x},\ E[C|r] = e^{\alpha+\beta r_c}$$

where α is a function of the mean and standard deviation of the prior:

$$\alpha = (1 - \beta)[\mu + (1/2)\sigma^2]$$

(Rational) participants will choose the risky option if and only if $p \times E[X|r] > E[C|r]$ or, equivalently, $\log\ p + \beta r_x > \beta r_c$, or $\log\ p + \beta r_x - \beta r_c > 0$ Since both r_x and r_c are (independent) Gaussian random variables, conditional on X and C, their difference is a Gaussian variable as well:

$$r_x - r_c \sim N(\log X - \log C,\ 2\nu^2)$$

Crucially, this means that the probability that the participants chooses the risky option ($\log\ p + \beta r_x - \beta r_c > 0$) conditional on C and X can be described using the cumulative normal distribution $\Phi(x)$:

$$\Phi\left(-\frac{\beta^{-1}\log p^{-1} - \log(X/C)}{\sqrt{2}\cdot\nu}\right)$$

The likelihood of the KLW model is equivalent to that of a Generalized Linear Model (GLM) with the Normal CDF Φ as the link function and a Bernoulli error distribution (probit model; see Ref. 120). Such a GLM can be fitted using of-the-shelf functions in most standard

statistical modelling software. When using a GLM-approach, the choice of the risky option is the dependent variable and an intercept (all 1's) regressor and $\log(X/C)$ as a regressor. Crucially, the resulting intercept parameter δ and slope parameter γ from the probit model can then be re-expressed in the parameters of the KLW model:

$$\gamma = \frac{1}{\sqrt{2}\nu}, \delta = \frac{\beta^{-1}\log p^{-1}}{\sqrt{2}\nu}$$

Parameter estimation

We fitted the psychometric model using the Bayesian hierarchical GLM-estimation package Bambi[123]. The standard probit model assumes that choices are determined by a fixed effect of both an intercept (determining the risk aversion) and the log ratio of the risky and safe option. We also estimate participants-wise random effects on all parameters so we had participants-wise KLW parameters:

$$p(risky_choice) \sim \Phi(\beta_0 + \beta_1 \log\frac{X}{C} + (\beta_{2,i} + \beta_{3,i}\log\frac{X}{C}))$$

Where β_0 and β_1 are fixed effects and $\beta_{2,i}$ and $\beta_{3,i}$ are random (participant-specific) effects.

or, in the formula-syntax of lme4/bambi:

risky_choice ~ 1 + log_risky_safe_order + (1 + log_risky_safe_|participant_id)

For some analyses in which we wanted to see how risk preferences are modulated for different contexts, we also included the order and/or the value of the safe option in the model as independent variables, so:

risky_choice ~ 1 + log_risky_safe_order*n_safe + (1 + log_risky_safe_*order*n_safe|participant_id.

Note that the point-of-indifference of the probit model is a function of both the intercept δ and slope parameter γ ($-\frac{\delta}{\gamma}$). To meaningfully quantify the point-of-indifference, we used the risk-neutral-probability (RNP)[43,50]. This is the hypothetical probability of the risky option

for which a risk-neutral decision-maker would show the same point-of-indifference as the participants. Thus, any RNP above 55% implies risk-seeking, whereas any RNP below 55% implies risk aversion. We defined participants as being risk-averse when the 95% Credible Interval of their RNP was below .55, and risk-seeking if the CI was above .55. When the CI overlapped with .55, we categorised participants as risk-neutral.

The risk neutral probability can be derived from the slope γ and intercept δ as follows:

$$\exp(-\frac{\delta}{\gamma})$$

To fit the hierarchical probit/KLW model, we used the standard weakly informative priors as implemented by default in the Bambi (based on the approach of the well-known *rstanarm*-package) package[123]. Briefly, the priors are Gaussian distributions centred at 0, with as a standard deviation 2.5 times the ratio between the standard deviation of the dependent and independent variable[123]. To sample from the parameter posteriors, we used the no U-Turn sampler (NUTS), which is a self-tuning version of the Hammiltonian MCMC sampler and is particularly efficient for high-dimensional models with correlations between the parameter, such as our model here[124]. We collected 4 chains of 2000 samples each (1000 burnin). We always visually inspected the traces of the NUTS sampler and made sure the Gelman-Rubin statistic was below 1.05 for all parameters.

PMC model

Model specification

Our Perceptual Memory-based Risky Choice model (PMCM) assumes that participants base their risky choices on noisy representations of the payoffs and choose the one with the largest expected payoff on a particular trial. Crucially, in the PMCM, the noisiness of the representation may depend on the order of presentation:

$$r_{x,1} \sim N(\log X, \nu_1^2), r_{x,2} \sim N(\log X, \nu_2^2)$$
$$r_{c,1} \sim N(\log C, \nu_1^2), r_{c,2} \sim N(\log C, \nu_2^2)$$

Where $r_{x,1}$ pertains to the representation of the payoff of the risky option presented first, $r_{x,2}$ to the representation of the payoff of a risky option presented second, $r_{c,1}$ to the

representation of the payoff of a safe option presented first, and $r_{c,2}$ to the payoff of a safe option presented second. Note that the noisiness of the risky and safe options ν_i is the same, only order of presentation influence noisiness. We expected that the noise for the first option ν_1 will be higher than that of the second option ν_2, but this is not enforced anywhere in the model (e.g., they have identical priors in the estimation procedure).

The PMCM also assumes that participants (potentially) employ different priors for the risky and safe payoffs, because these payoffs come from objectively different distributions:

$$\log X \sim N(\mu_x, \sigma_x^2), \log C \sim N(\mu_c, \sigma_c^2)$$

For a given parameter set $[\nu_1, \nu_2, \mu_x, \mu_c, \sigma_x, \sigma_c]$ and objective payoffs X and C, we can now obtain the distribution of the expectations of the participants for the two options, which is the product of the prior and evidence distributions and follows a normal distribution (in logarithmic space) :

$$E[\log X|r] \sim N(r_x + \frac{\nu_i^2}{\nu_i^2+\sigma_x^2}\cdot(\mu_x - r_x), \nu_i^2)$$

$$E[\log C|r] \sim N(r_c + \frac{\nu_i^2}{\nu_i^2+\sigma_c^2}\cdot(\mu_c - r_c), \nu_i^2)$$

Thus, the distribution of differences between these expectations in log space is given by the difference of these two distributions, $E[\log X|r]$ - $E[\log C|r]$, which is also a normal distribution:

$$E[\log X|r] - E[\log C|r] \sim N(\delta, \sigma')$$

with

$$\delta = r_x + \frac{\nu_i^2}{\nu_i^2+\sigma_x^2}\cdot(\mu_x - X) - (r_c + \frac{\nu_i^2}{\nu_i^2+\sigma_c^2}\cdot\left(\mu_c - r_c\right))$$

and

$$\varsigma^2 = \nu_1^2+\nu_2^2$$

The likelihood of choosing the risky option according to the PMCM is defined as the probability that the participant's estimate of the difference between the risky and safe option ($E[\log X|r] - E[\log C|r]$) is larger than the payout probability of the risky option in log space:

$$p(E[\log X|r] + \log p > E[\log C]) = \Phi(\frac{\log p + \delta}{\varsigma})$$

Where $\Phi(x)$ is the standard cumulative normal distribution.

Model estimation

We implemented the PMCM using the Bayesian statistical modelling library pymc (v.5)[125] and wrapped it in our Python package *bauer*[1]. We used a hierarchical (regression) approach for estimation. This means that for all main six parameters of the model $[\nu_1, \nu_2, \mu_x, \mu_c, \sigma_x, \sigma_c]$, we assume a group distribution which is a Gaussian distribution. Furthermore, for the ν- and σ-parameters, which are necessarily non-negative, we estimated transformed parameters in an unrestricted space $[-\infty, \infty]$ which we then transformed into the non-negative domain $[0, \infty]$ using the softplus function $\log(1 + \exp(x))$.

For a given parameter θ (e.g., ν_1 or σ_x), the participants-specific parameter of participants p was a linear combination of the mean group parameter μ_θ plus an individually-determined offset-parameter δ_θ times the standard deviation of the group distribution σ_θ:

$$\theta_p = \mu_\theta + \delta_\theta \cdot \sigma_\theta$$

This offset-based specification of the hierarchical model was chosen to prevent the likelihood "funnels" that plague high-dimensional hierarchical models[126].

When relating the PMCM parameters to neural measures, we used a regression approach[70], where a given parameter θ_p (e.g., ν_1 or σ_x) of participants p on a trial t was a linear sum of both an intercept θ_0 and a regression coefficient θ_n times the neural measure at trial t, n_t:

$$\theta_{p,t} = \theta_{p,0} + \theta_{p,n} \cdot n_{p,t}$$

We used mildly informative priors on all group distribution parameters:

For the evidence parameters:

$$\mu_{\nu_1}, \mu_{\nu_2} \sim N(-1, 0.5) \text{ (before softplus transformation)}$$

For the mean of the prior on risky payoffs:

$$\mu_{\mu_x} \sim N(\hat{\mu}_x, 0.5)$$

Where $\hat{\mu}_x$ is the *objective* mean of the payoffs of risky options (in log space)

[1] https://github.com/ruffgroup/bauer/

For the mean of the prior on safe payoffs:

$$\mu_{\mu_c} \sim N(\hat{\mu}_c,\ 0.5)$$

Where $\hat{\mu}_x$ is the *objective* mean of the payoffs of safe options (in log space)

For the standard deviation of the priors:

$$\mu_{\sigma_x}, \mu_{\sigma_c} \sim N(0,\ 0.5) \text{ (before softplus transformation)}$$

The regression coefficient on (z-scored) neural measures was a Gaussian centred at 0 with a standard deviation of 1:

$$\mu_{\theta_n} \sim N(0,\ 1.)$$

The prior on all group variance parameters was a Half-Cauchy parameter [127]:

$$\sigma_{\nu_1},\ \sigma_{\nu_2}, \sigma_{\mu_x}, \sigma_{\mu_c},\ \sigma_{\sigma_x}, \sigma_{\sigma_c},\ \sigma_{\theta_n} \sim halfCauchy(0.25)$$

Posterior estimates were obtained using the NUTS-sampler as implemented in pymc 5 using a target acceptatnce rate of 90%. We obtained 4 chains with 3000 samples each (1500 burnin). If we encountered divergences, we increased the target acceptance rate to 92.5%.

To obtain estimates of the size and presence of an effect, we used "Bayesian" p-values –the probability mass of the posterior estimate above/below 0[128]. We generally used one-tailed cutoffs of 5% probability mass.

Model comparisons were performed using the estimated log pointwise predictive density (ELPD[ELPD; 60]) which is a state-of-the art model comparison technique that – unlike other information theoretic measures like BIC and DIC – takes into account the shape of the posterior distribution and the *effective* number of parameters of the model.

MRI parameters

3T

We acquired functional MRI data using the Philips Achieva 3T whole-body MR scanner equipped with a 32-channel MR head coil, located at the Laboratory for Social and Neural Systems Research (SNS-Lab) of the UZH Zurich Center for Neuroeconomics. We collected

8 runs of fMRI data with a T2*-weighted gradient-recalled echo-planar imaging (GR-EPI) sequence (150 volumes + 5 dummies; flip angle 90 degrees; TR = 2286 ms, TE = 30ms; matrix size 96 × 70, FOV 240 × 175mm; in-plane resolution of 2.5 mm; 39 slices with thickness of 2.5 mm and a slice gap of 0.5mm; SENSE acceleration in phase-encoding direction (left-right) with factor 1.5; time-of-acquisition 4:52 minutes). Additionally, we acquired high-resolution T1weighted 3D MPRAGE image (FOV: 256 × 256 × 170 mm; resolution 1 mm isotropic; TI = 2800 ms; 256 shots, flip angle 8 degrees; TR = 8.0 ms; TE = 3.7 ms; SENSE acceleration in left-right direction 2; time-of-acquisition 5:35 minutes).

7T

We also acquired MRI data using a Philips Achieva 7T whole-body MR scanner (located at the Institute for Biomedical Technology of ETH Zurich) equipped with: 7T MRI quadrature transmit/32-channel head receive array coil (Nova Medical). For the functional data, we acquired T2*-weighed GRE-EPI sequences (150 volumes + 5 dummies); flip angle 74 degrees, TR=2300 ms; TE = 15ms; matrix size 109 x 128; FOV 190 x 224 mm; in-plane resolution of 1.75 mm; 76 slices with thickness of 1.75 mm with no slice gap; SENSE-acceleration in phase-encoding direction (left-right) with factor 3; Multiband acceleration with factor 2; time-of-acquisition 5:35 minutes). At the 7T, acquired a T1-weighted 3D MPRAGE image (FOV: 240 x 240 x 160 mm; resolution 0.8 x 1.0 x 0.8 mm; TI = 3000 ms; 164 shots; flip angle 7 degrees; TR = 9.8 ms; TE = 4.5 ms; SENSE acceleration in left-right direction 3; in anterior-posterior direction 1.5; time-of-acquisition: 4:43 minutes).

fMRI preprocessing

Preprocessing on fMRI data was performed using fMRIPrep 20.2.2 [129], which is based on Nipype 1.6.1 [130,131].

Anatomical data preprocessing

The T1-weighted (T1w) images collected from the 3T and 7T data were processed together. All of them were corrected for intensity non-uniformity (INU) with N4BiasFieldCorrection [132], distributed with ANTs 2.3.3 [133]. The T1w-reference was then skull-stripped with a Nipype implementation of the antsBrainExtraction.sh workflow (from ANTs), using OASIS30ANTs as

target template. Brain tissue segmentation of cerebrospinal fluid (CSF), white-matter (WM) and gray-matter (GM) was performed on the brain-extracted T1w using fast [FSL 5.0.9; ,134]. A T1w-reference map was computed after registration of 3 T1w images (after INU-correction) using mri_robust_template [FreeSurfer 6.0.1 135]. Brain surfaces were reconstructed using recon-all [FreeSurfer 6.0.1; ,136], and the brain mask estimated previously was refined with a custom variation of the method to reconcile ANTs-derived and FreeSurfer-derived segmentations of the cortical gray-matter of Mindboggle [137]. Volume-based spatial normalization to one standard space (MNI152NLin2009cAsym) was performed through nonlinear registration with antsRegistration (ANTs 2.3.3), using brain-extracted versions of both T1w reference and the T1w template. The following template was selected for spatial normalization: ICBM 152 Nonlinear Asymmetrical template version 2009c [138],

Functional data preprocessing

For each of the 24 BOLD runs found per participants (across all tasks and sessions), the following preprocessing was performed. First, a reference volume and its skull-stripped version were generated using a custom methodology of fMRIPrep. BOLD runs were slice-time corrected using 3dTshift from AFNI 20160207 [139]. Head-motion parameters with respect to the BOLD reference (transformation matrices, and six corresponding rotation and translation parameters) are estimated before any spatiotemporal filtering using mcflirt [FSL 5.0.9; ,140]. A B0-nonuniformity map (or fieldmap) was estimated based on two (or more) echo-planar imaging (EPI) references with opposing phase-encoding directions, with 3dQwarp [139] (AFNI 20160207). Based on the estimated susceptibility distortion, a corrected EPI (echo-planar imaging) reference was calculated for a more accurate co-registration with the anatomical reference. The BOLD reference was then co-registered to the T1w reference using bbregister (FreeSurfer) which implements boundary-based registration [141]. Co-registration was configured with six degrees of freedom. The BOLD time-series (including slice-timing correction when applied) were resampled onto their original, native space by applying a single, composite transform to correct for head-motion and susceptibility distortions. These resampled BOLD time-series will be referred to as preprocessed BOLD in original space, or just preprocessed BOLD. The BOLD time-series were resampled onto the following surfaces (FreeSurfer reconstruction nomenclature): fsaverage, fsnative. Several confounding time-series were calculated based on the preprocessed BOLD: framewise displacement (FD), DVARS and three region-wise global

signals. FD was computed using two formulations following Power [absolute sum of relative motions, 142] and Jenkinson (relative root mean square displacement between affines, [140]. FD and DVARS are calculated for each functional run, both using their implementations in Nipype (following the definitions by Power et al. 2014). The three global signals are extracted within the CSF, the WM, and the whole-brain masks. Additionally, a set of physiological regressors were extracted to allow for component-based noise correction [CompCor, 143]. Principal components are estimated after high-pass filtering the preprocessed BOLD time-series (using a discrete cosine filter with 128s cut-off) for the two CompCor variants: temporal (tCompCor) and anatomical (aCompCor). tCompCor components are then calculated from the top 2% variable voxels within the brain mask. For aCompCor, three probabilistic masks (CSF, WM and combined CSF+WM) are generated in anatomical space. The implementation differs from that of Behzadi et al. in that instead of eroding the masks by 2 pixels on BOLD space, the aCompCor masks are subtracted a mask of pixels that likely contain a volume fraction of GM. This mask is obtained by dilating a GM mask extracted from the FreeSurfer's aseg segmentation, and it ensures components are not extracted from voxels containing a minimal fraction of GM. Finally, these masks are resampled into BOLD space and binarized by thresholding at 0.99 (as in the original implementation). Components are also calculated separately within the WM and CSF masks. For each CompCor decomposition, the k components with the largest singular values are retained, such that the retained components' time series are sufficient to explain 50 percent of variance across the nuisance mask (CSF, WM, combined, or temporal). The remaining components are dropped from consideration. The head-motion estimates calculated in the correction step were also placed within the corresponding confounds file. The confound time series derived from head motion estimates and global signals were expanded with the inclusion of temporal derivatives and quadratic terms for each [144]. Frames that exceeded a threshold of 0.5 mm FD or 1.5 standardised VARS were annotated as motion outliers. The BOLD time-series were resampled into standard space, generating a preprocessed BOLD run in MNI152NLin2009cAsym space. First, a reference volume and its skull-stripped version were generated using a custom methodology of fMRIPrep. All resamplings can be performed with a single interpolation step by composing all the pertinent transformations (i.e. head-motion transform matrices, susceptibility distortion correction when available, and co-registrations to anatomical and output spaces). Gridded (volumetric) resamplings were performed using antsApplyTransforms (ANTs), configured with Lanczos interpolation to

minimize the smoothing effects of other kernels [145]. Non-gridded (surface) resamplings were performed using mri_vol2surf (FreeSurfer). First, a reference volume and its skull-stripped version were generated using a custom methodology of fMRIPrep. BOLD runs were slice-time corrected using 3dTshift from AFNI 20160207 [139]. The BOLD reference was then co-registered to the T1w reference using bbregister (FreeSurfer) which implements boundary-based registration [141]. Co-registration was configured with six degrees of freedom. The BOLD time-series (including slice-timing correction when applied) were resampled onto their original, native space by applying the transforms to correct for head-motion. These resampled BOLD time-series will be referred to as preprocessed BOLD in original space, or just preprocessed BOLD. The BOLD time-series were resampled onto the following surfaces (FreeSurfer reconstruction nomenclature): fsaverage, fsnative. The BOLD time-series were also resampled into standard space, generating a preprocessed BOLD run in MNI152NLin2009cAsym space.

Many internal operations of fMRIPrep use Nilearn 0.6.2 [146], mostly within the functional processing workflow. For more details of the pipeline, see the section corresponding to workflows in fMRIPrep's documentation.

fMRI analyses

The main goal of our fMRI analyses was to get a trialwise estimate of the fidelity of the representation of payoff magnitudes in the numerical parietal cortex[50]. Following earlier work[50,52,53], we used an encoding/decoding-modelling approach, where we inverted an encoding model that describes how a voxel i responds to specific stimulus magnitude s $f(s) \rightarrow x_i$ in a Bayesian framework, by extending the encoding model to a multivariate likelihood function $p(X|s)$ using a multivariate t-distribution: $[x_1, .., x_n] \sim f_{1..n}(s) + \epsilon$ with $\epsilon \sim t(0, \Sigma, d)$, where Σ is the residual covariance and d is the degrees-of-freedom of the t-distribution. Using an explicit likelihood function allows us to decode from trial-to-trial what was the presented payoff magnitude, as well as the fidelity of the neural response. For every trial, we test the consistency of the BOLD activation pattern for all possible numerosities. The fidelity of the neural response was operationalised as the dispersion (standard deviation) of the decoded posterior. Loosely speaking, the posterior will be less dispersed when the BOLD responses of many voxels agree with a small set of numerosities. When the amplitude of the response across voxels is smaller and/or they are not consistent

with the same numerosities, the posterior will be more dispersed, as the decoder is less certain about which stimulus was presented. We postulate, as other have done before[52,53], that the uncertainty of our decoding of the presented stimulus is related to the fidelity of the *neural representation* of that stimulus.

The main fMRI analysis can roughly be split up in the following steps: 1) Fit a single-trial GLM to estimate trialwise measures of the response amplitude across voxels 2) Fit a numerical receptive field model[54] to the response, 3) Fit a multivarite noise model to the residuals of the nPRF model in a leave-one-run-out cross-validation scheme[53] 4) Obtain a posterior estimate of the payoffs magnitudes of unseen data using the noise model and an inverted nPRF model.

Single trial estimates

We used the GLMSingle Python package[147] to obtain single-trial BOLD estimates. Briefly, the GLMSingle package uses cross-validation to do model selection over GLMs with a) a library of different hemodynamic response functions b) different L2-regularisation parameters to shrink the single trial estimates, combating the issue of correlated single trial regressors[148]. c) GLMSingle also obtains GLMDenoise[149] regressors based on the first *n* PCA components in a set of noise voxels. Noise voxels are defined as having low explained variance in the task-based GLM. The number of PCA components is selected via cross-validation.

As input to GLMSingle, we used both the 24 first and 24 second payoff presentations per run. For the second payoff pesentations, we modeled all trials with the same numerosity as being in the same condition, to aid GLMSingle with cross-validation (similar numerosities should have similar responses). After extensive analysis piloting, we chose to not include any additional confound regressors (e.g. motion parameters, RETROICOR parameters or aCompCorr regressros) in addition to the GLMDenoise confound regressors, as additional regressors did not lead to robustly increased (or even decreased) decoding accuracy and GLMDenoise. This is in line with earlier work on GLMDenoise[149] and the related aCompCorr approach[143].

Numerical receptive field modelling

We fitted a numerical receptive field model to all voxels in the brain, for each session separately (so using 192 single trial estimates). The method is described in detail

elsewhere[50,54], so we only briefly describe it here. First, we estimate the mean μ, standard deviation σ, amplitude A and baseline B of a log-normal receptive field for every voxel in the brain separately, to predict the BOLD response of these voxels to different numerosities.

$$f_i(x) = B_i + A_i \exp\left(-\left(\log x - \left(\log \frac{\mu_i}{1+\sigma_i^2/\mu_i^2}\right)\right)^2 / \left(2\log\left(1+\sigma_i^2/\mu_i\right)\right)\right)$$

The second part of this equation is a parameterisation of the log-normal probability density function where μ and σ are the mean and standard deviation of the distribution in natural space. Although this parameterisation is somewhat exotic, it is highly useful when plotting the estimated preferred numerosities and their dispersion, for example on the cortical surface.

We first fit the model by using a grid-search: We correlatethe single trial estimates for the first payoff stimulus presentation with the predictions of a large grid of 60 μ-s between 5 and 80 and 60 σ-s between 5 and 40. We then estimate I and A linear least-squares on the best-correlating μ and σ-parameters. Finally, we used gradient descent[150] to refine parameters further. The explained variance R^2 for each voxel is then transformed to *fsaverage*-surface space to compare across participants. We compared the R^2-maps to an ROI of the (right) numerical parietal cortex (rNPC) in *fsaverage* we drew for an earlier study. We observed that the R^2-maps were tightly related to the (see Figure 2) and therefore chose to use this rNPC-mask in all follow-up analyses. The rNPC mask was transformed from *fsaverage*-surface space to individual anatomical space using *neuropythy* (https://github.com/noahbenson/neuropythy).

Voxel selection

One key methodological choice in the encoding/decoding-framework is which voxels to include in the decoding step. In earlier work we chose an arbitrary number of voxels/surface vertices[50]. Although the number of voxels seemed to make little difference in individual decoding accuracy, it remains an arbitrary choice. Here, we chose to use a nested cross-validation scheme to select the number of voxels for each participants/run in a principled way. The method takes into account both that noisy voxels should have an out-of-sample R^2 lower than 0 and different brains have different sizes. Specifically, when decoding run i (out of a total of 8 runs per session), we would fit the nPRF model on all voxels within the NPC mask on (6-run) subsets of the remaining 7 runs, by leaving another run j out $R_{_i_j}$. Then, for each of these nested folds $R_{_i_j}$, we calculated the *out-of-sample* R^2

on run j for each voxel. Thus, for each voxel and each decoded test run i, we had 6 out-of-sample $R^2 s$, which we averaged over. For decoding run i, we would only use voxels that had a mean out-of-sample R^2 larger than 0.

Decoding

After voxel selection, we used a leave-one-run-out cross validation scheme where the nPRF model was fitted to all runs but the test run, after which also a multivariate noise model was fitted to the residual signals. Specifically, we fitted the following covariance matrix:

$$\Sigma = \rho\tau\tau^T + (1 - \rho)I \circ \tau\tau^T + \sigma WW^T,$$

as well as the degrees-of-freedom of a 0-centred, multivariate t-distribution. Briefly, τ is a vector as its length the number of voxels (n) in the ROI. It pertains to the standard deviation of the residuals of each voxel. Thus, ρ determines to which extent all voxels correlate with each other ($\tau\tau^T$ is the covariance matrix of perfectly correlated voxels, whereas $I \circ \tau\tau^T$ corresponds to a perfectly diagonal matrix/spherical covariance). W is a square matrix of $n \times n$. Each element $W_{i,j}$ is the product of the receptive fields of voxels i and j across stimulus space $(f_i(S)\, f_j(S))^T$ with S being the entire stimulus space $[5, 6, .., 112]$. Thus, the free scalar parameter σ determines to which extent voxels with overlapping receptive fields have more correlated noise.

Once the noise model is fitted, we can now determine a likelihood function for any multivariate BOLD pattern X and for any numerical stimulus s:

$$p(X|s) = t(X - [f_1, f_2, ..., f_n(s)], \Sigma, d)$$

Since we assume a flat prior on all integers between 5 and 112, we can now just evaluate this likelihood on all these integers and normalize the resulting probability mass function (pdf) to integrate to 1. We take the expected value of this pdf to be our estimate of the presented stimulus. We take the standard deviation of the pdf as a measure of the fidelity of neural coding. This standard deviation is used to split up trial within a participants and payoff-numerosity for the probit model and as input to the PMCM as a linear regressor on all the model parameters.

Code availability

All the code used in this package can be found online on github:
https://github.com/Gilles86/risk_experiment/

Our computational cognitive models are implemented in the open-source Python library *bauer*
https://github.com/ruffgroup/bauer/tree/main

The used nPRF model and decoding software algorithms are implemented in the open-source Python library *braincoder*
https://braincoder-devs.github.io/

References

1. Mas-Colell, A., Whinston, M. D. & Green, J. R. Microeconomic Theory. (Oxford University Press, New York, 1995).
2. Stigler, G. J. & Becker, G. S. De Gustibus Non Est Disputandum. The American Economic Review 67, 67–90 (1977).
3. Morgenstern, O. & Neumann, J. V. Theory of Games and Economic Behavior. (Princeton University Press, Princeton, NJ, 1947).
4. Kahneman, D. & Tversky, A. Prospect Theory: An Analysis of Decision under Risk. Econometrica 47, 363–391 (1979).
5. Bruhin, A., Fehr-Duda, H. & Epper, T. Risk and Rationality: Uncovering Heterogeneity in Probability Distortion. Econometrica 78, 1375–1412 (2010).
6. Pedroni, A. et al. The risk elicitation puzzle. Nat Hum Behav 1, 803–809 (2017).
7. Hey, J. D. & Orme, C. Investigating Generalizations of Expected Utility Theory Using Experimental Data. Econometrica 62, 1291 (1994).
8. Frey, R., Pedroni, A., Mata, R., Rieskamp, J. & Hertwig, R. Risk preference shares the psychometric structure of major psychological traits. Sci Adv 3, e1701381 (2017).
9. Mata, R., Frey, R., Richter, D., Schupp, J. & Hertwig, R. Risk Preference: A View from Psychology. J. Econ. Perspect. 32, 155–172 (2018).
10. J, D. T. et al. Individual risk attitudes: measurement, determinants and behavioral consequences. Journal of the European Economic Association 9, 522–550 (2009).
11. Bernoulli, D. Specimen theoriae novae de mensura sortis (Exposition of a New Theory on the Measurement of Risk). Papers Imp. Acad. Sci. St. Petersburg 5, 175–192 (1738).
12. Becker, G. S. A Treatise on the Family: Enlarged Edition. (Harvard University Press, 1993).
13. Friedman, M. Theory of the Consumption Function. (Princeton university press, 1957).
14. Sloan, F. A. & Hsieh, C.-R. Health Economics. (MIT Press, 2017).
15. Tietenberg, T. & Lewis, L. Environmental and Natural Resource Economics. (Routledge, 2018).
16. Bodie, Z., Kane, A. & Marcus, A. Essentials of Investments. (McGraw Hill, 2013).
17. Fehr, E. & Schmidt, K. M. A Theory of Fairness, Competition, and Cooperation. Q. J. Econ. 114, 817–868 (1999).
18. Dilaver, Ö., Jump, R. C. & Levine, P. Agent-Based Macroeconomics and Dynamic Stochastic General Equilibrium Models: Where Do We Go from Here? J. Econ. Surv. 32, 1134–1159 (2018).
19. Fehr, E. & Tyran, J.-R. Individual Irrationality and Aggregate Outcomes. JEP 19, 43–66 (2005).
20. Siegrist, M., Cvetkovich, G. & Gutscher, H. Risk Preference Predictions and Gender Stereotypes. Organ. Behav. Hum. Decis. Process. 87, 91–102 (2002).
21. Huettel, S. A., Stowe, C. J., Gordon, E. M., Warner, B. T. & Platt, M. L. Neural Signatures of Economic Preferences for Risk and Ambiguity. Neuron 49, 765–775 (2006).
22. Louie, K. & Glimcher, P. W. Separating Value from Choice: Delay Discounting Activity in the Lateral Intraparietal Area. J. Neurosci. 30, 5498–5507 (2010).

23. Chew, B. et al. Endogenous fluctuations in the dopaminergic midbrain drive behavioral choice variability. PNAS 116, 18732–18737 (2019).
24. Weber, E. U. Risk attitude and preference. Wiley Interdiscip. Rev.: Cogn. Sci. 1, 79–88 (2010).
25. Chuang, Y. & Schechter, L. Stability of experimental and survey measures of risk, time, and social preferences: A review and some new results. J. Dev. Econ. 117, 151–170 (2015).
26. Schildberg-Hörisch, H. Are Risk Preferences Stable? J. Econ. Perspect. 32, 135–154 (2018).
27. Walasek, L. & Stewart, N. How to Make Loss Aversion Disappear and Reverse: Tests of the Decision by Sampling Origin of Loss Aversion. J Exp Psychology Gen 144, 7–11 (2015).
28. Molter, F. & Mohr, P. N. C. Presentation order but not duration affects binary risky choice. (2021) doi:10.31234/osf.io/gcthj.
29. Woodford, M. Modeling Imprecision in Perception, Valuation, and Choice. Annu. Rev. Econ. 12, 1–23 (2020).
30. Mosteller, F. & Nogee, P. An Experimental Measurement of Utility. J. Political Econ. 59, 371–404 (1951).
31. McFadden, D. Conditional Logit Analysis of Qualitative Choice Behavior. in Frontiers in Econometrics (ed. Zarembka, P.) 105–142 (Academic Press, 1973).
32. McFadden, D. L. Econometric analysis of qualitative response models. in Handbook of Econometrics vol. 2 1395–1457 (1984).
33. Shadlen, M. N. & Shohamy, D. Decision Making and Sequential Sampling from Memory. Neuron 90, 927–939 (2016).
34. Busemeyer, J. R., Gluth, S., Rieskamp, J. & Turner, B. M. Cognitive and Neural Bases of Multi-Attribute, Multi-Alternative, Value-based Decisions. TiCS 23, 251–263 (2019).
35. Heng, J. A., Woodford, M. & Polania, R. Efficient sampling and noisy decisions. eLife 9, e54962 (2020).
36. Faisal, A. A., Selen, L. P. J. & Wolpert, D. M. Noise in the nervous system. Nat Rev Neurosci 9, 292–303 (2008).
37. Petzschner, F. H., Glasauer, S. & Stephan, K. E. A Bayesian perspective on magnitude estimation. TiCS 19, 285–293 (2015).
38. Lieder, F. & Griffiths, T. L. Resource-rational analysis: understanding human cognition as the optimal use of limited computational resources. Behav Brain Sci 43, 1–85 (2019).
39. Wei, X.-X. & Stocker, A. A. A Bayesian observer model constrained by efficient coding can explain “anti-Bayesian” percepts. Nat Neurosci 18, 1509–1517 (2015).
40. Weber, E. U. Perception matters: Psychophysics for economists. in The Psychology of Economic Decisions: Reasons And Choices vol. 2 163–176 (Oxford Academic, 2004).
41. Slovic, P. Perception of risk. Science 236, 280–285 (1987).
42. Slovic, P. The Construction of Preference. American Psychologist 50, 364–371 (1995).
43. Khaw, M. W., Li, Z. & Woodford, M. Cognitive Imprecision and Small-Stakes Risk Aversion. Rev Econ Stud 88, 1979–2013 (2020).
44. Vieider, F. M. Noisy coding of time and reward discounting. (2021).
45. Vieider, Ferdinand M. Noisy Neural Coding and Decisions under Uncertainty. (2021).
46. Frydman, C. & Jin, L. J. Efficient Coding and Risky Choice. Q J Econ 137, 161–213

(2021).
47. Ma, W. J., Beck, J. M., Latham, P. E. & Pouget, A. Bayesian inference with probabilistic population codes. Nat Neurosci 9, 1432–1438 (2006).
48. Barlow, H. B. Possible Principles Underlying the Transformations of Sensory Messages. in Sensory Communication 216–234 (1961). doi:10.7551/mitpress/9780262518420.003.0013.
49. Hollingworth, H. L. The Central Tendency of Judgment. J. Philos., Psychol. Sci. Methods 7, 461 (1910).
50. Barretto-García, M. et al. Individual risk attitudes arise from noise in neurocognitive magnitude representations. Nat. Hum. Behav. 7, 1551–1567 (2023).
51. Newsome, W. T., Britten, K. H. & Movshon, J. A. Neuronal correlates of a perceptual decision. Nature 341, 52–54 (1989).
52. Walker, E. Y., Cotton, R. J., Ma, W. J. & Tolias, A. S. A neural basis of probabilistic computation in visual cortex. Nat Neurosci 23, 122–129 (2020).
53. Bergen, R. S. van, Ma, W. J., Pratte, M. S. & Jehee, J. F. M. Sensory uncertainty decoded from visual cortex predicts behavior. Nat Neurosci 18, 1728 (2015).
54. Harvey, B. M., Klein, B. P., Petridou, N. & Dumoulin, S. O. Topographic Representation of Numerosity in the Human Parietal Cortex. Science 341, 1123–1126 (2013).
55. Honig, M., Ma, W. J. & Fougnie, D. Humans incorporate trial-to-trial working memory uncertainty into rewarded decisions. Proc National Acad Sci 117, 8391–8397 (2020).
56. Ma, W. J., Husain, M. & Bays, P. M. Changing concepts of working memory. Nat Neurosci 17, 347–356 (2014).
57. Bays, P. M., Schneegans, S., Ma, W. J. & Brady, T. F. Representation and computation in visual working memory. Nat. Hum. Behav. 8, 1016–1034 (2024).
58. Gaudecker, H.-M. von, Soest, A. van & Wengström, E. Heterogeneity in Risky Choice Behavior in a Broad Population. Am. Econ. Rev. 101, 664–694 (2011).
59. Gelman, A. et al. Bayesian Data Analysis. (Chapman and Hall/CRC, 2013).
60. Vehtari, A., Gelman, A. & Gabry, J. Practical Bayesian model evaluation using leave-one-out cross-validation and WAIC. Stat Comput 27, 1413–1432 (2017).
61. Yao, Y., Vehtari, A., Simpson, D. & Gelman, A. Using Stacking to Average Bayesian Predictive Distributions. Bayesian Anal. 13, (2017).
62. Waschke, L., Tune, S. & Obleser, J. Local cortical desynchronization and pupil-linked arousal differentially shape brain states for optimal sensory performance. Elife 8, e51501 (2019).
63. Beaman, C. B., Eagleman, S. L. & Dragoi, V. Sensory coding accuracy and perceptual performance are improved during the desynchronized cortical state. Nat Commun 8, 1308 (2017).
64. Ringach, D. L. Spontaneous and driven cortical activity: implications for computation. Curr. Opin. Neurobiol. 19, 439–444 (2009).
65. Harris, K. D. & Thiele, A. Cortical state and attention. Nat Rev Neurosci 12, 509–523 (2011).
66. Bergen, R. S. van & Jehee, J. F. M. Probabilistic Representation in Human Visual Cortex Reflects Uncertainty in Serial Decisions. J Neurosci 39, 8164–8176 (2019).

67. Britten, K. H., Newsome, W. T., Shadlen, M. N., Celebrini, S. & Movshon, J. A. A relationship between behavioral choice and the visual responses of neurons in macaque MT. Vis. Neurosci. 13, 87–100 (1996).
68. Purushothaman, G. & Bradley, D. C. Neural population code for fine perceptual decisions in area MT. Nat. Neurosci. 8, 99–106 (2005).
69. Lasne, G., Piazza, M., Dehaene, S., Kleinschmidt, A. & Eger, E. Discriminability of numerosity-evoked fMRI activity patterns in human intra-parietal cortex reflects behavioral numerical acuity. Cortex 114, 90–101 (2019).
70. Wiecki, T. V., Sofer, I. & Frank, M. J. HDDM: Hierarchical Bayesian estimation of the Drift-Diffusion Model in Python. Front Neuroinform 7, 14 (2013).
71. Cavanagh, J. F. et al. Subthalamic nucleus stimulation reverses mediofrontal influence over decision threshold. Nat. Neurosci. 14, 1462–1467 (2011).
72. Olschewski, S. & Rieskamp, J. Distinguishing three effects of time pressure on risk taking: Choice consistency, risk preference, and strategy selection. J. Behav. Decis. Mak. 34, 541–554 (2021).
73. Olschewski, S., Rieskamp, J. & Scheibehenne, B. Taxing Cognitive Capacities Reduces Choice Consistency Rather Than Preference: A Model-Based Test. J Exp Psychology Gen 147, 462–484 (2018).
74. Olschewski, S., Rieskamp, J. & Hertwig, R. The link between cognitive abilities and risk preference depends on measurement. Sci. Rep. 13, 21151 (2023).
75. Vieider, F. M. Decisions Under Uncertainty as Bayesian Inference on Choice Options. Manag. Sci. (2024) doi:10.1287/mnsc.2023.00265.
76. Oprea, R. Decisions Under Risk are Decisions Under Complexity. AER (2024).
77. Manzini, P. & Mariotti, M. Welfare economics and bounded rationality: the case for model-based approaches. J. Econ. Methodol. 21, 343–360 (2014).
78. Dehaene, S. The Number Sense: How the Mind Creates Mathematics. (Oxford University Press, 2011).
79. Tsetsos, K., Chater, N. & Usher, M. Salience driven value integration explains decision biases and preference reversal. Proc National Acad Sci 109, 9659–9664 (2012).
80. Prat-Carrabin, A. & Woodford, M. Efficient coding of numbers explains decision bias and noise. Nat Hum Behav 6, 1142–1152 (2022).
81. Cai, Y., Hofstetter, S. & Dumoulin, S. O. Nonsymbolic Numerosity Maps at the Occipitotemporal Cortex Respond to Symbolic Numbers. The J. Neurosci. 43, 2950–2959 (2023).
82. Krajbich, I., Armel, C. & Rangel, A. Visual fixations and the computation and comparison of value in simple choice. Nat Neurosci 13, 1292–1298 (2010).
83. Krajbich, I. Accounting for attention in sequential sampling models of decision making. Curr Opin Psychology 29, 6–11 (2018).
84. Smith, S. M. & Krajbich, I. Gaze Amplifies Value in Decision Making. Psychol. Sci. 30, 116–128 (2018).
85. Ma, W. J. Bayesian Decision Models: A Primer. Neuron 104, 164–175 (2019).
86. Khaw, M. W., Glimcher, P. W. & Louie, K. Normalized value coding explains dynamic adaptation in the human valuation process. Proc National Acad Sci 114, 12696–12701

(2017).
87. Levy, D. J. & Glimcher, P. W. The root of all value: a neural common currency for choice. Curr Opin Neurobiol 22, 1027–1038 (2012).
88. Hayden, B. Y. & Niv, Y. The Case Against Economic Values in the Orbitofrontal Cortex (or Anywhere Else in the Brain). Behav Neurosci 135, 192–201 (2021).
89. O'Doherty, J. P. The problem with value. Neurosci Biobehav Rev 43, 259–268 (2014).
90. Forstmann, B. U., Wagenmakers, E.-J., Eichele, T., Brown, S. & Serences, J. T. Reciprocal relations between cognitive neuroscience and formal cognitive models: opposites attract? Trends Cogn Sci 15, 272–279 (2011).
91. Glimcher, P. W. & Fehr, E. Neuroeconomics: Decision Making and the Brain. (Academic Press, 2013).
92. Gold, J. I. & Shadlen, M. N. The Neural Basis of Decision Making. Annu. Rev. Neurosci. 30, 535–574 (2007).
93. Polanía, R., Krajbich, I., Grueschow, M. & Ruff, C. C. Neural Oscillations and Synchronization Differentially Support Evidence Accumulation in Perceptual and Value-Based Decision Making. Neuron 82, 709–720 (2014).
94. Polanía, R., Moisa, M., Opitz, A., Grueschow, M. & Ruff, C. C. The precision of value-based choices depends causally on fronto-parietal phase coupling. Nat Commun 6, 8090 (2015).
95. Platt, M. L. & Glimcher, P. W. Neural correlates of decision variables in parietal cortex. Nature 400, 233–238 (1999).
96. Louie, K., Grattan, L. E. & Glimcher, P. W. Reward value-based gain control: divisive normalization in parietal cortex. J Neurosci Official J Soc Neurosci 31, 10627–39 (2011).
97. Coutlee, C. G., Kiyonaga, A., Korb, F. M., Huettel, S. A. & Egner, T. Reduced Risk-Taking following Disruption of the Intraparietal Sulcus. Front Neurosci-switz 10, 588 (2016).
98. Panidi, K., Vorobiova, A. N., Feurra, M. & Klucharev, V. Posterior parietal cortex is causally involved in reward valuation but not in probability weighting during risky choice. Cereb. Cortex 34, bhad446 (2023).
99. Foucault, C. et al. A nonlinear code for event probability in the human brain. bioRxiv 2024.02.28.582455 (2024) doi:10.1101/2024.02.28.582455.
100. Hayden, B. Y. & Moreno-Bote, R. A neuronal theory of sequential economic choice. Brain Neurosci Adv 2, 2398212818766675 (2018).
101. Zhang, Z., Yin, C. & Yang, T. Evidence accumulation occurs locally in the parietal cortex. Nat. Commun. 13, 4426 (2022).
102. Griffiths, T. L., Lieder, F. & Goodman, N. D. Rational Use of Cognitive Resources: Levels of Analysis Between the Computational and the Algorithmic. Topics in Cognitive Science 7, 217–229 (2015).
103. Mackowiak, B., Matejka, F. & Wiederholt, M. Rational Inattention: A Review. CEPR Discussion Papers (2020).
104. Hollander, G. de, Forstmann, B. U. & Brown, S. D. Different Ways of Linking Behavioral and Neural Data via Computational Cognitive Models. Biological Psychiatry Cognitive Neurosci Neuroimaging 1, 101–109 (2016).
105. Khaw, M. W., Li, Z. & Woodford, M. Cognitive Imprecision and Stake-Dependent Risk

Attitudes. SSRN Electron. J. (2022) doi:10.2139/ssrn.4210005.
106. Gershman, S. J. & Bhui, R. Rationally inattentive intertemporal choice. Nat Commun 11, 3365 (2020).
107. Gabaix, X. & Laibson, D. Myopia and Discounting. (2017).
108. Hu, J., Konovalov, A. & Ruff, C. C. A unified neural account of contextual and individual differences in altruism. eLife 12, e80667 (2023).
109. Walker, D. M. Gambling, Consumer Behavior, and Welfare. in Casinomics (ed. Walker, D. M.) 19–24 (2013).
110. Marfels, C. Is Gambling Rational? The Utility Aspect of Gambling. Gaming Law Rev. 5, 459–466 (2001).
111. Brown, R. I. F. Arousal and Sensation-Seeking Components in the General Explanation of Gambling and Gambling Addictions. Int. J. Addict. 21, 1001–1016 (1986).
112. FeldmanHall, O., Glimcher, P., Baker, A. L. & Phelps, E. A. Emotion and Decision-Making Under Uncertainty: Physiological Arousal Predicts Increased Gambling During Ambiguity but Not Risk. J. Exp. Psychol.: Gen. 145, 1255–1262 (2016).
113. Krishnamurthy, K., Nassar, M. R., Sarode, S. & Gold, J. I. Arousal-related adjustments of perceptual biases optimize perception in dynamic environments. Nat Hum Behav 1, 0107 (2017).
114. Griffiths, M. D. The cognitive psychology of gambling. J. Gambl. Stud. 6, 31–42 (1990).
115. Spurrier, M. & Blaszczynski, A. Risk Perception in Gambling: A Systematic Review. J. Gambl. Stud. 30, 253–276 (2014).
116. Rogers, P. The Cognitive Psychology of Lottery Gambling: A Theoretical Review. J. Gambl. Stud. 14, 111–134 (1998).
117. Paliwal, S., Petzschner, F. H., Schmitz, A. K., Tittgemeyer, M. & Stephan, K. E. A model-based analysis of impulsivity using a slot-machine gambling paradigm. Front. Hum. Neurosci. 8, 428 (2014).
118. Paliwal, S. et al. Subjective estimates of uncertainty during gambling and impulsivity after subthalamic deep brain stimulation for Parkinson's disease. Sci. Rep. 9, 14795 (2019).
119. Alserda, G. A. G., Dellaert, B. G. C., Swinkels, L. & Lecq, F. S. G. van der. Individual pension risk preference elicitation and collective asset allocation with heterogeneity. J Bank Financ 101, 206–225 (2019).
120. Stewart, N., Canic, E. & Mullett, T. L. On the futility of estimating utility functions: Why the parameters we measure are wrong, and why they
do not generalize. PsyArXiv (2019) doi:10.31234/osf.io/qt69m.
121. Miedl, S. F., Peters, J. & Büchel, C. Altered Neural Reward Representations in Pathological Gamblers Revealed by Delay and Probability Discounting. Arch. Gen. Psychiatry 69, 177–186 (2012).
122. Cobb-Clark, D. A., Dahmann, S. C. & Kettlewell, N. Depression, Risk Preferences and Risk-Taking Behavior. SSRN Electron. J. (2019) doi:10.2139/ssrn.3390275.
123. Capretto, T. et al. Bambi: A simple interface for fitting Bayesian linear models in Python. arXiv (2020) doi:10.48550/arxiv.2012.10754.
124. Hoffman, M. D. & Gelman, A. The No-U-Turn Sampler: Adaptively Setting Path Lengths in Hamiltonian Monte Carlo. Journal of Machine Learning Research 15, 1593–1623 (2011).

125. Patil, A., Huard, D. & Fonnesbeck, C. J. PyMC: Bayesian Stochastic Modelling in Python. J. Stat. Softw. 35, 1–81 (2010).
126. Betancourt, M. J. & Girolami, M. Hamiltonian Monte Carlo for Hierarchical Models. arXiv 79, 2–4 (2015).
127. Gelman, A. Prior distributions for variance parameters in hierarchical models (comment on article by Browne and Draper). Bayesian Anal 1, 515–534 (2006).
128. Kruschke, J. K. Doing Bayesian Data Analysis: A Tutorial with R and BUGS. (Academic Press., Burlington, MA, 2011).
129. Esteban, O. et al. fMRIPrep: a robust preprocessing pipeline for functional MRI. Nat Methods 16, 111–116 (2019).
130. Gorgolewski, K. J. et al. Nipype. Software. Zenodo. https://doi. org/10.5281/zenodo 596855, (2018).
131. Gorgolewski, K. et al. Nipype: A Flexible, Lightweight and Extensible Neuroimaging Data Processing Framework in Python. Frontiers Neuroinformatics 5, 13 (2011).
132. Tustison, N. J. et al. N4ITK: Improved N3 Bias Correction. IEEE Trans. Méd. Imaging 29, 1310–1320 (2010).
133. Avants, B. B., Tustison, N. & Song, G. Advanced normalization tools (ANTS). 2, (2009).
134. Zhang, Y., Brady, M. & Smith, S. Segmentation of Brain MR Images Through a Hidden Markov Random Field Model and the Expectation-Maximization Algorithm. IEEE Trans. Méd. Imaging 20, 45 (2001).
135. Reuter, M., Rosas, H. D. & Fischl, B. Highly accurate inverse consistent registration: A robust approach. NeuroImage 53, 1181–1196 (2010).
136. Dale, A. M., Fischl, B. & Sereno, M. I. Cortical Surface-Based Analysis I. Segmentation and Surface Reconstruction. Neuroimage 9, 179–194 (1999).
137. Klein, A. et al. Mindboggling morphometry of human brains. PLoS Comput. Biology 13, e1005350 (2017).
138. Fonov, V., Evans, A., McKinstry, R., Almli, C. & Collins, D. Unbiased nonlinear average age-appropriate brain templates from birth to adulthood. NeuroImage 47, S102 (2009).
139. Cox, R. W. & Hyde, J. S. Software tools for analysis and visualization of fMRI data. NMR Biomed. 10, 171–178 (1997).
140. Jenkinson, M., Bannister, P., Brady, M. & Smith, S. Improved optimization for the robust and accurate linear registration and motion correction of brain images. Neuroimage 17, 825–841 (2002).
141. Greve, D. N. & Fischl, B. Accurate and robust brain image alignment using boundary-based registration. 48, (2009).
142. Power, J. D. et al. Methods to detect, characterize, and remove motion artifact in resting state fMRI. NeuroImage 84, 320–341 (2014).
143. Behzadi, Y., Restom, K., Liau, J. & Liu, T. T. A component based noise correction method (CompCor) for BOLD and perfusion based fMRI. NeuroImage 37, 90–101 (2007).
144. Satterthwaite, T. D. et al. An improved framework for confound regression and filtering for control of motion artifact in the preprocessing of resting-state functional connectivity data. NeuroImage 64, 240–256 (2013).
145. Lanczos, C. Evaluation of Noisy Data. J. Soc. Ind. Appl. Math. Ser. B Numer. Anal. 1,

76–85 (1964).
146. Abraham, A. et al. Machine learning for neuroimaging with scikit-learn. Frontiers Neuroinformatics 8, 14 (2014).
147. Prince, J. S. et al. Improving the accuracy of single-trial fMRI response estimates using GLMsingle. Elife 11, e77599 (2022).
148. Mumford, J. A., Turner, B. O., Ashby, F. G. & Poldrack, R. A. Deconvolving BOLD activation in event-related designs for multivoxel pattern classification analyses. NeuroImage 59, 2636–2643 (2012).
149. Kay, K. N., Rokem, A., Winawer, J., Dougherty, R. F. & Wandell, B. A. GLMdenoise: a fast, automated technique for denoising task-based fMRI data. Front. Neurosci. 7, 247 (2013).
150. Kingma, D. P. & Ba, J. Adam: A Method for Stochastic Optimization. arXiv (2014) doi:10.48550/arxiv.1412.6980.

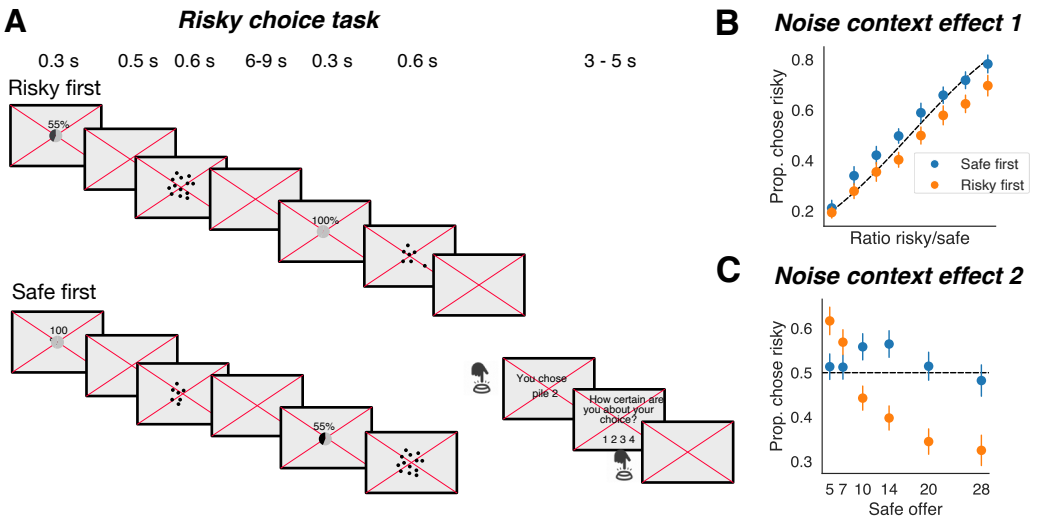
A
Risky choice task
0.3 s
0.5 s
0.6 s
6-9 s
0.3 s
0.6 s
3 - 5 s
Risky first
55%
100%
Safe first
100
55%
You chose pile 2
How certain are you about your choice?
1 2 3 4
B
Noise context effect 1
Prop. chose risky
0.8
0.6
0.4
0.2
Safe first
Risky first
Ratio risky/safe
C
Noise context effect 2
Prop. chose risky
0.6
0.5
0.4
0.3
5 7 10 14 20 28
Safe offer

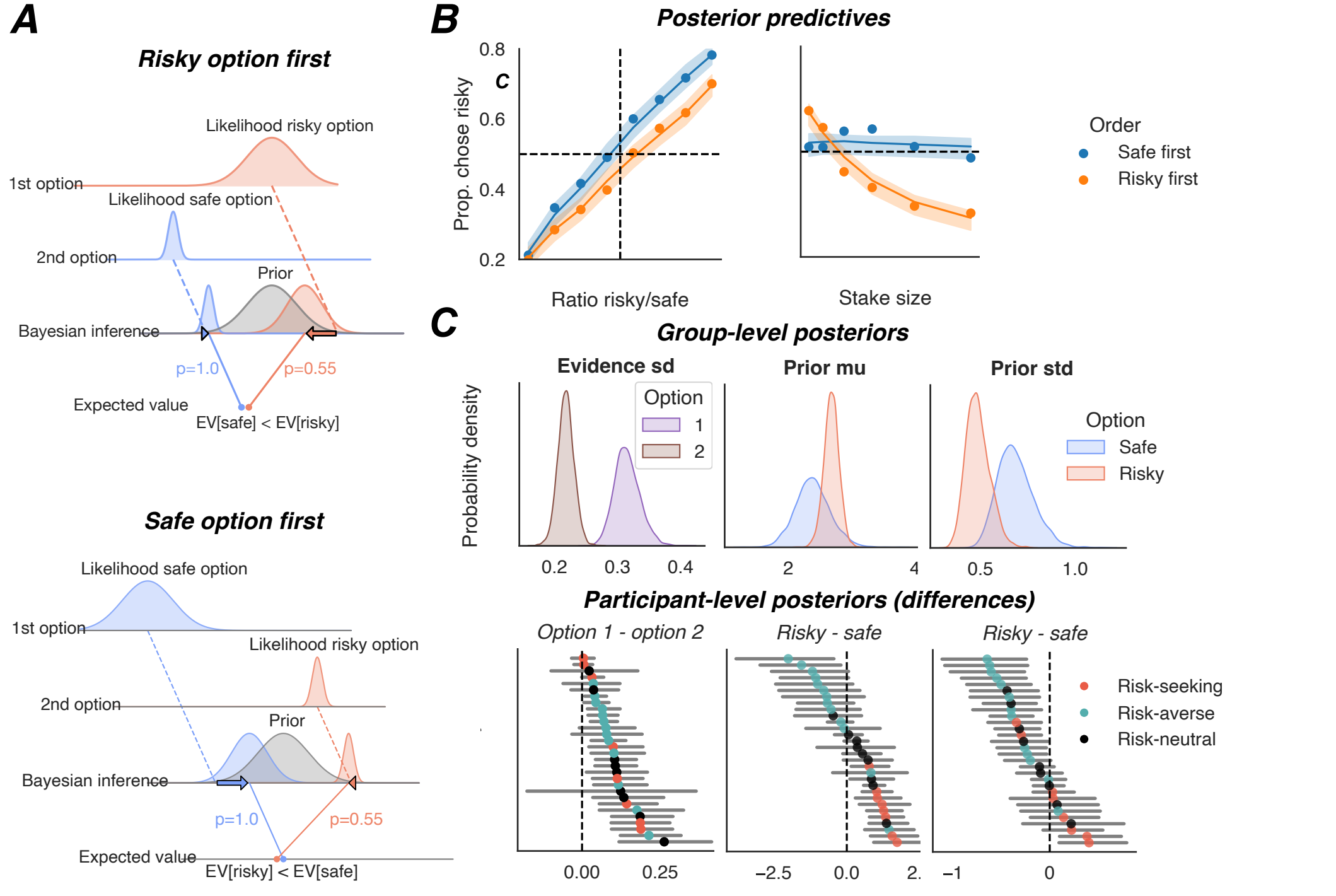
A
Risky option first
Likelihood risky option
1st option
Likelihood safe option
2nd option
Prior
Bayesian inference
p=1.0
p=0.55
Expected value
EV[safe] < EV[risky]
Safe option first
Likelihood safe option
1st option
Likelihood risky option
2nd option
Prior
Bayesian inference
p=1.0
p=0.55
Expected value
EV[risky] < EV[safe]
B
Posterior predictives
Prop. chose risky
0.8
0.6
0.4
0.2
Ratio risky/safe
Stake size
Order
Safe first
Risky first
C
Group-level posteriors
Probability density
Evidence sd
Option
1
2
0.2
0.3
0.4
Prior mu
2
4
Prior std
0.5
1.0
Option
Safe
Risky
Participant-level posteriors (differences)
Option 1 - option 2
0.00
0.25
Risky - safe
−2.5
0.0
2.
Risky - safe
−1
0
Risk-seeking
Risk-averse
Risk-neutral

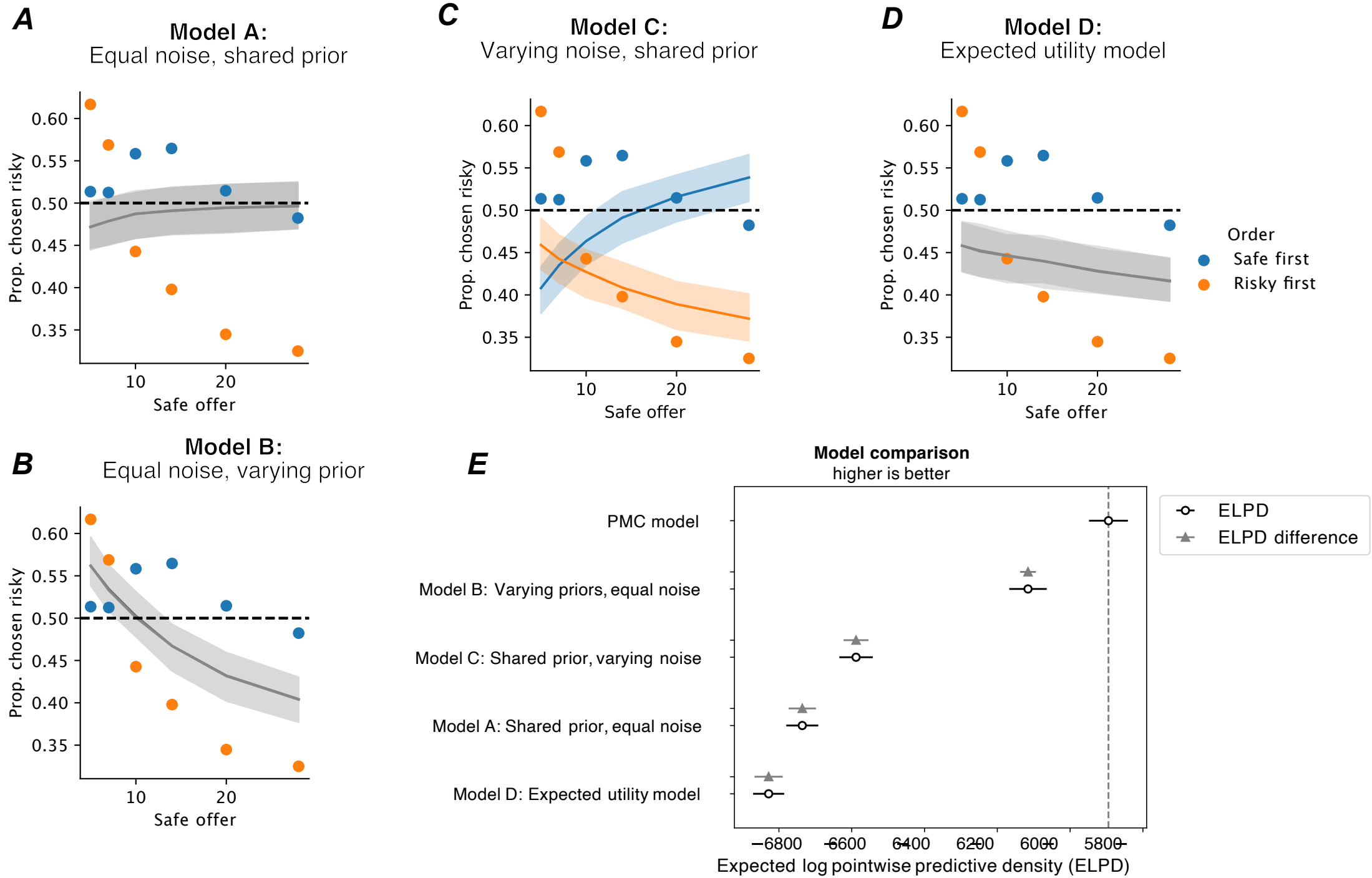
A
Model A:
Equal noise, shared prior
C
Model C:
Varying noise, shared prior
D
Model D:
Expected utility model
B
Model B:
Equal noise, varying prior
E
Model comparison
higher is better
Prop. chosen risky
Safe offer
0.60
0.55
0.50
0.45
0.40
0.35
10
20
Order
Safe first
Risky first
ELPD
ELPD difference
PMC model
Model B: Varying priors, equal noise
Model C: Shared prior, varying noise
Model A: Shared prior, equal noise
Model D: Expected utility model
−6800
−6600
−6400
−6200
−6000
−5800
Expected log pointwise predictive density (ELPD)

A Non-linear numerosity tuning in parietal cortex

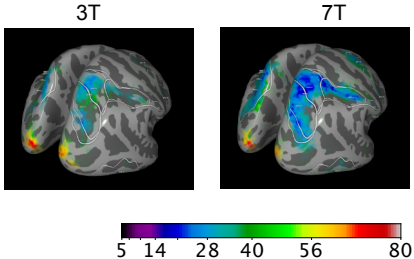

B Numerosity can be reliably decoded

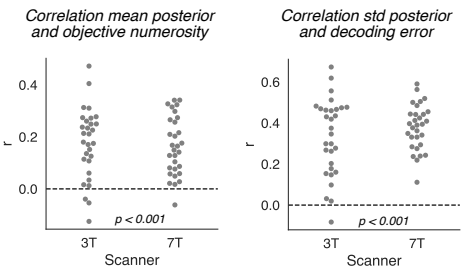

C Noisier neural signals shift risk preferences away from risk-neutral

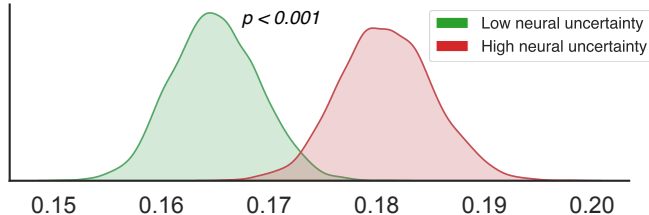

D Decoded uncertainty is related to the noisiness of the representation of the first option
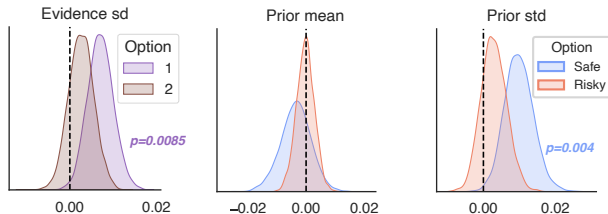
Posterior of group parameter estimates of model regressors on neural uncertainty